iScience

CellPress
OPEN ACCESS

Article

MLL5 is involved in retinal photoreceptor maturation through facilitating CRX-mediated photoreceptor gene transactivation

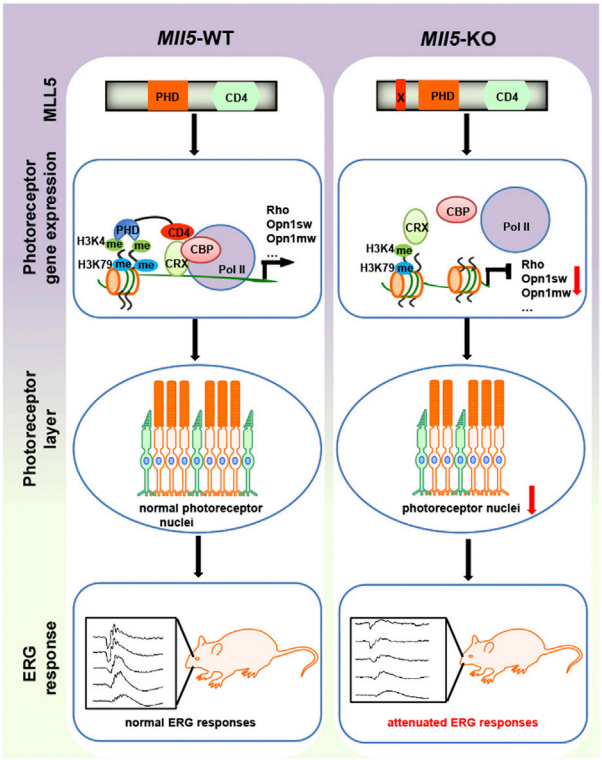

Xiaoming Zhang, Bo-Wen Zhang, Lue Xiang, ..., Yan Zhang, Zi-Bing Jin, Lih-Wen Deng

jinzb502@ccmu.edu.cn (Z.-B.J.)
bchdlw@nus.edu.sg (L.-W.D.)

Highlights

MLL5 is essential for the expression of critical photoreceptor genes

MLL5 depletion reduces H3K4/K79 methylation at photoreceptor gene promoters

MLL5 interacts with CRX via its CD4 domain

Recognition of H3K4me2/3 by MLL5 is a prerequisite for CRX recruitment to chromatin

Zhang et al., iScience *25*, 104058
April 15, 2022
https://doi.org/10.1016/j.isci.2022.104058

iScience

CellPress
OPEN ACCESS

Article

MLL5 is involved in retinal photoreceptor maturation through facilitating CRX-mediated photoreceptor gene transactivation

Xiaoming Zhang,[1,2] Bo-Wen Zhang,[3,4] Lue Xiang,[3] Hui Wu,[1] SUPIT Alva Sahiri Alexander,[5] Peipei Zhou,[6] Melvin Zi-Yu Dai,[1] Xiaoyun Wang,[7] Wenjun Xiong,[5] Yan Zhang,[8] Zi-Bing Jin,[7,*] and Lih-Wen Deng[1,9,10,11,12,*]

SUMMARY

Histone methylation, particularly at the H3K4 position, is thought to contribute to the specification of photoreceptor cell fate; however, the mechanisms linking histone methylation with transcription factor transactivation and photoreceptor gene expression have not yet been determined. Here, we demonstrate that MLL5 is abundantly expressed in the mouse retina. Mll5 deficiency impaired electroretinogram responses, alongside attenuated expression of a number of retina genes. Mechanistic studies revealed that MLL5 interacts with the retina-specific transcription factor, CRX, contributing to its binding to photoreceptor-specific gene promoters. Moreover, depletion of MLL5 impairs H3K4 methylation and H3K79 methylation, which subsequently compromises CRX-CBP assembly and H3 acetylation on photoreceptor promoters. Our data support a scenario in which recognition of H3K4 methylation by MLL5 is required for photoreceptor-specific gene transcription through maintaining a permissive chromatin state and proper CRX-CBP recruitment at promoter sites.

INTRODUCTION

The vertebrate retina comprises six major types of neurons (cone, rod, bipolar, amacrine, horizontal, and ganglion cells) and one type of glial cells (Müller glia) derived from a common population of multipotent progenitor cells that develop in a conserved order. The transition of progenitor cells into terminally differentiated retinal cells is accompanied by repression of progenitor cell-related genes and upregulation of genes specific for retinal cell types. Emerging evidence suggests that histone methylation in the developing retina is dynamically regulated and contributes to retinal differentiation in a lineage-specific manner. Proper retinal-terminal differentiation requires precise methylation of H3K9/27 and H3K4, which are predominantly correlated with gene repression and activation, respectively (Iwagawa and Watanabe, 2019; Raeisossadati et al., 2021). Previous genome-wide analyses of retinal methylation profiles using chromatin immunoprecipitation sequencing (ChIP-seq) have shown that rod photoreceptor differentiation is accompanied by *de novo* H3K4me2/3 accumulation around the transcription starting sites (TSS) and gene bodies of a subset of rod photoreceptor-specific genes, which correlates with their increased gene expression (Popova et al., 2012; Ueno et al., 2016). However, the action of H3K4me2/3 on photoreceptor-specific gene activation remains unclear.

Histone methylations can serve as signals for the recruitment of distinct "reader" proteins to alter chromatin accessibility. For instance, H3K4me3, which is enriched at active promoters, can recruit chromatin-modifying factors, such as histone acetyltransferases, resulting in histone acetylation and gene activation. Moreover, H3K4 methylation may contribute to transcription initiation via recruitment of basal transcription machinery or tethering of specific transcription factors to target gene promoters. Detectable H3K4me3 has been found at active enhancers bound by RNA polymerase II (Pol II) (Calo and Wysocka, 2013). However, it is unclear how H3K4me2/3 signals are transduced to transcription machinery that are subsequently recruited to specific photoreceptor genes during retinal development. Previous studies have determined a series of transcription factors that execute essential roles in photoreceptor development and maintenance (Hennig et al., 2008; Swaroop et al., 2010). CRX (cone-rod homeobox protein) is known as a key transcription factor for photoreceptor gene transcription (Furukawa et al., 1997, 1999). A crucial function of CRX is to recruit HAT-containing coactivators to photoreceptor gene chromatin for histone acetylation (Peng

[1]Department of Biochemistry, Yong Loo Lin School of Medicine (YLLSOM), National University of Singapore, Singapore 117597, Singapore

[2]NHC Key Laboratory of Research on Quality and Standardization of Biotech Products, National Institutes for Food and Drug Control, Beijing 102629, China

[3]Laboratory for Stem Cell & Retinal Regeneration, Institute of Stem Cell Research, The Eye Hospital, Wenzhou Medical University, Wenzhou 325027, China

[4]Shanghai Institute of Nutrition and Health, Chinese Academy of Sciences, Shanghai 200031, China

[5]Department of Biomedical Sciences, City University of Hong Kong, Hong Kong SAR, China

[6]Department of Immunology, St. Jude Children's Research Hospital, Memphis, TN 38105, USA

[7]Beijing Institute of Ophthalmology, Beijing Tongren Eye Center, Beijing Tongren Hospital, Capital Medical University, Beijing Ophthalmology and Visual Sciences Key Laboratory, Beijing 100730, China

[8]Shanghai General Hospital, Shanghai Jiao Tong University School of Medicine, Shanghai 201620, China

[9]National University Cancer Institute, Singapore National University Health System (NUHS), Singapore 119074, Singapore

[10]NUS Center for Cancer Research, YLLSOM, NUS, Singapore 117599, Singapore

[11]NUS Graduate School - Integrative Sciences and Engineering Programme,

Continued

and Chen, 2007). Recent study demonstrated that CRX is required for chromatin remodeling at specific target sites, which undergo retina or neuronal specific activation during photoreceptor differentiation (Ruzycki et al., 2018). CRX is expressed originally in photoreceptor precursors that are localized to the gene-rich euchromatin regions of the rod photoreceptor nuclei (Corbo et al., 2010; Popova et al., 2012; Solovei et al., 2009), where H3K4me2/3 markers are also highly enriched during retinal development (Rao et al., 2010). It is largely undetermined whether H3K4me2/3 are required for CRX function.

High levels of transcription have been linked to a high degree of H3K79 methylation, which typically peak around the transcription start site (TSS) with diminished levels throughout genes (Bernt et al., 2011; Steger et al., 2008). Importantly, H3K79 methylation has been linked to embryonic development, haematopoiesis, cardiac function, and the development of leukemia (Ljungman et al., 2019; Nguyen and Zhang, 2011), whereas H3K79 methylation in the regulation of retinal photoreceptor maturation and integrity has not been investigated. H3K79 methylation is present in the promoter and coding regions of active genes, suggesting a role for H3K79 methylation in transcription activation and elongation (Wood et al., 2018). Although the mechanism by which H3K79 methylation regulates transcription is largely undetermined, H3K79 may act through recruiting or repelling effector proteins (Vlaming and van Leeuwen, 2016). It has also been suggested that H3K79 methylation may inhibit chromatin localization of repressors, thereby maintaining an open chromatin state with elevated H3K9 acetylation and H3K79 methylation (Chen et al., 2015). It is of note that the patterning of H3K79 methylation and H3K4 methylation shows several similarities in mammalian chromatin (Steger et al., 2008). High H3K4 and H3K79 methylation and H3 acetylation are required for the recognition and binding of c-Myc to target genes (Guccione et al., 2006). Moreover, H2BK123 ubiquitination by Rad6 (ubiquitin-conjugating E2 enzyme) and Bre1 (ubiquitin E3 ligase) is a prerequisite for both H3K4 and H3K79 methylation (Shahbazian et al., 2005); however, whether H3K4 and H3K79 methylation are linked in the transcriptional regulation of photoreceptor genes is still unclear.

Methylation of H3K4 is known to be catalyzed by the SET (Su(var)three to nine, Enhancer-of-zeste, and Trithorax) domain containing histone methyltransferases (HMT), which are conserved from yeast to humans. In mammalian cells, the MLL (or KMT2) family consists of seven members, including MLL1-5 (KMT2A-2E), SET1A (KMT2F), and SET1B (KMT2G). MLL1 has been reported to play a cell type-specific role in retinal development at multiple levels that differs from other histone modifying enzymes, such as EED and EZH2 in the polycomb repressive complex 2 (RPC2) (Brightman et al., 2018). A recent study showed that SET1A played pivotal roles for the survival and proliferation of retinal progenitors via H3K4 modifications of Uhrf1 (Deng et al., 2021). MLL5 (also known as KMT2E) consists of a single N-terminal SET domain and a plant homeodomain (PHD) zinc finger (Zhang et al., 2017). Although the function of the MLL5 PHD finger as a molecular reader of H3K4me2/3 has been well-documented, the role of MLL5 as an epigenetic modifying factor remains controversial following several reports demonstrating that recombinant MLL5 lacks intrinsic HMT activity. Although the MLL5 splice variant has been reported to exhibit *in vitro* H3K4 tri-methylation activity (Nin et al., 2015), it remains unclear whether MLL5 possesses cell type or cell context-dependent HMT activity. MLL5 has been reported to be essential for cell cycle progression and genomic stability maintenance (Zhao et al., 2016). Previous studies of *Mll5*-deficient mice have demonstrated a requirement for MLL5 in hematopoiesis and spermatogenesis, as well as in the immune system (Zhang et al., 2017). Here, we demonstrate that MLL5 is highly expressed in the mouse retina and is essential for visual function. MLL5 facilitates the establishment of proper methylation of H3K4 and H3K79 at photoreceptor gene promoters. Moreover, MLL5 associates with CRX, which subsequently recruits CBP and promotes a permissive chromatin state for photoreceptor gene transactivation.

RESULTS

MLL5 is abundantly expressed in the mouse retina

Previous RNA tissue arrays indicated that MLL5 is highly expressed in fetal thymus and kidney and in adult hematopoietic tissues, jejunum, and cerebellum (Emerling et al., 2002). We wondered whether elevated expression of MLL5 is responsible for cell type or cell context-dependent activity. To identify additional MLL5 expression cells or tissues, we searched the Single-cell RNA-seq data of the Single Cell Portal database (https://singlecell.broadinstitute.org/single_cell) in 340 total studies collected by the Broad Institute. Using this approach, we found that 197 studies showed expression of the MLL family genes with different patterns in different cell types. Interestingly, MLL5 expression is the highest compared to other members of the MLL family in all 10 retinal studies.

NUS, Singapore 119077, Singapore

[12]Lead contact

*Correspondence: jinzb502@ccmu.edu.cn (Z.-B.J.), bchdlw@nus.edu.sg (L.-W.D.)

https://doi.org/10.1016/j.isci.2022.104058

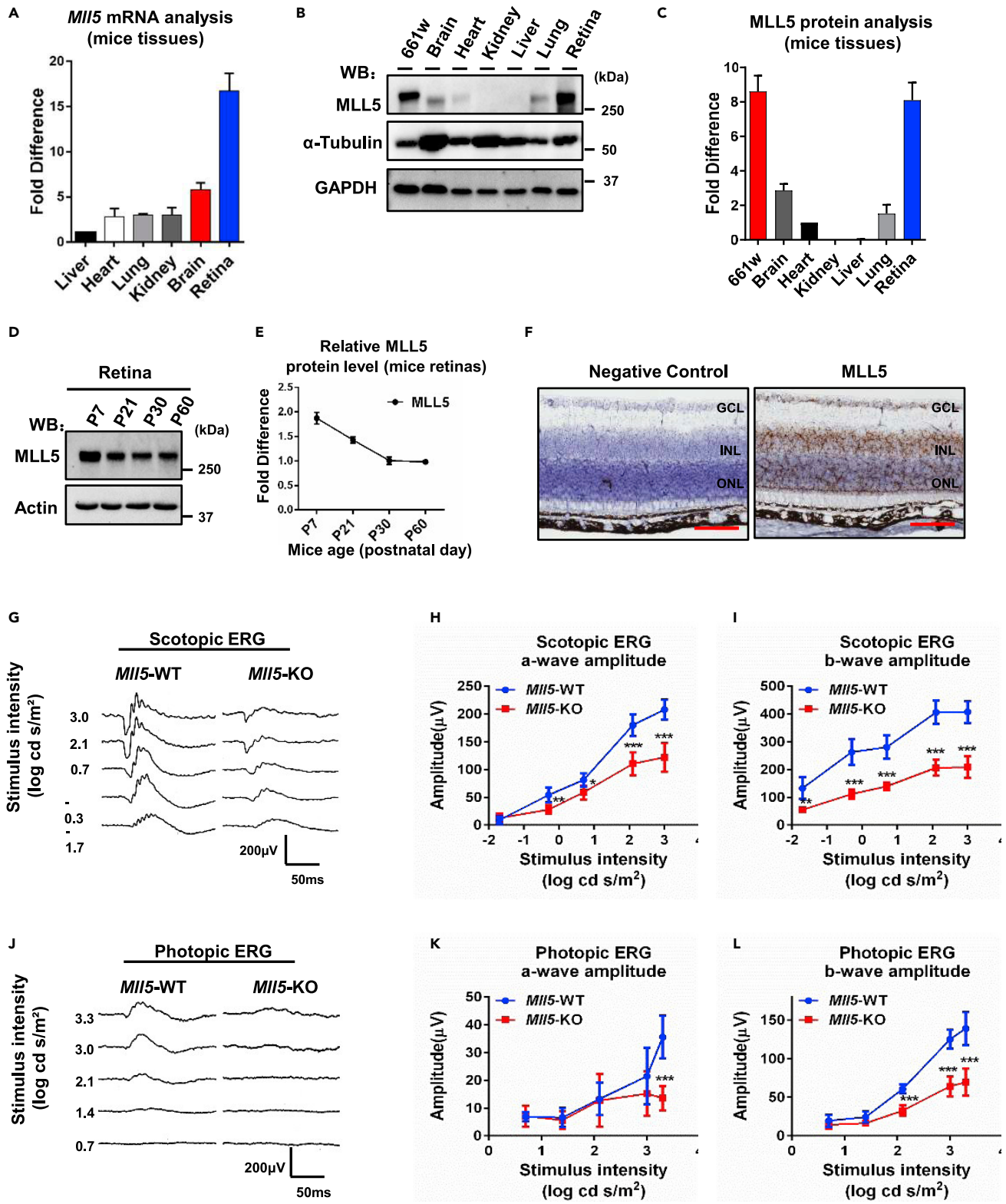

Figure 1. MLL5 is necessary for visual function of the mouse retina

(A) qPCR analysis of MLL5 transcripts in different mouse tissues (8-week-old) shows significantly higher expression in the retina compared with other tissues (normalized to the average ct values of reference genes *18S rRNA* and *β-actin*). Error bars represent SEM (n = 3).

Figure 1. *Continued*

(B) Representative western blotting of at least three experimental repeats shows enriched expression of MLL5 protein in the retina. Equivalent amounts of protein (20 μg) were loaded for each panel and probed with anti-MLL5, anti-α-Tubulin, or anti-GAPDH antibodies.

(C) Protein expression levels determined by western blotting in Figure 1B were quantified using Gel-Pro Analyzer (Version 4.0) software. MLL5 expression levels in the heart were set to 1. Error bars represent SEM (n = 3).

(D) MLL5 is broadly expressed in the retina during early development. Data shown are representative western blotting of at least three experimental repeats.

(E) Protein expression levels determined by western blotting in Figure 1D were quantified using Gel-Pro Analyzer (Version 4.0) software and normalized to actin expression. MLL5 expression levels in P60 retinas were set to 1. Error bars represent SEM (n = 3).

(F) *Mll5* mRNA was expressed in all nuclear layers at P21 mice retinas. *Mll5* mRNA expression was analyzed with Mll5 antisense probe and Mll5 sense probe (negative control) using *in situ* hybridization by RNAscope. Nuclear DNA was counterstained with hematoxylin. ONL, outer nuclear layer; INL, inner nuclear layer; GCL, ganglion cell layer. Scale bar, 50 μm.

(G–L) ERG analysis of *Mll5*-KO and control mice (n = 5 from each group). (G) Representative scotopic ERG elicited by five different stimulus intensities of white light was recorded. (H and I) The amplitudes of the scotopic ERG a-wave (H) and the b-wave (I), shown as a function of the stimulus intensity, were significantly reduced in *Mll5*-KO mice. (J) Representative photopic ERG elicited by five different stimulus intensities of white light is shown. (K) The amplitudes of the photopic ERG a-wave as a function of the stimulus intensity (3.3 log cd s/m^2) were significantly reduced in *Mll5*-KO mice. (L) The amplitudes of the photopic ERG b-wave are shown as a function of the stimulus intensity was significantly reduced in *Mll5*-KO mice. Error bars show the SEM (n = 5). *p < 0.05, **p < 0.01, ***p < 0.001, Student's t test.

To explore the potential involvement of MLL5 in retinal development and maintenance, we examined its expression pattern in murine retina. *Mll5* mRNA was ubiquitously expressed in all examined tissues of adult mice, consistent with previous reports (Emerling et al., 2002), but with highest *Mll5* mRNA expression level found in the retina (Figures 1A and S1A). Abundant MLL5 protein expression in the retina was confirmed by immunoblot (Figures 1B and 1C). We then examined MLL5 expression in the retina across various postnatal developmental stages. MLL5 protein was detected in developing retinas at P7 and P21 and at slightly lower levels in adult retinas at P30 and P60 (Figures 1D and 1E). However, we detected no significant differences in *Mll5* mRNA expression between developmental time points (Figure S1B), suggesting possible posttranscriptional regulation of MLL5 during retinal development. To investigate the spatial expression of MLL5 in the retina, we assessed *Mll5* mRNA expression by *in situ* hybridization (ISH) with *Mll5* antisense probe, and *Mll5* sense probe was used as the negative control. *Mll5* expression was observed in all nuclear layers of the dorsal retina and ventral retina at the age of P21 (Figures 1F and S1C). Given the abundant expression of MLL5 in the retina, we speculated that MLL5 may play a role in visual function.

Mll5-deficient mouse exhibit early-onset attenuated electroretinogram (ERG) responses

To investigate a possible role for MLL5 in visual function of retina, we conducted a morphological analysis of retinas from *Mll5*-KO mouse, which was generated by removing eight nucleotides from the third coding exon of the *Mll5* gene using CRISPR/Cas9 (Zhou et al., 2018). This allele results in a knockout of MLL5 protein by introducing a premature stop codon in exon three because of a frameshift. The absence of MLL5 protein in *Mll5*-KO retinas was confirmed by immunoblotting with anti-MLL5 antibody (Cheng et al., 2008) (Figure S1D). We analyzed *in vivo* scotopic (dark-adapted) and photopic (light-adapted) electroretinogram (ERG) responses in control and *Mll5*-KO mouse at P16. The scotopic ERG was elicited by five different light stimulus intensities (−1.7, −0.3, 0.7, 2.1, and 3.0 log cd s/m^2) (Figure 1G). The amplitude of the scotopic a-wave and b-wave, which originate from the activity of rod photoreceptors and rod bipolar cells, respectively, was significantly decreased in *Mll5*-KO mice at all light stimulus intensities (Figures 1H and 1I). The photopic ERG was also elicited using five different light stimulus intensities (0.7, 1.4, 2.1, 3.0, and 3.3 log cd s/m^2) (Figure 1J). The amplitude of the negative a-wave, which represents electrical potentials from cone photoreceptors, was significantly reduced at a high stimulus intensity of 3.3 log cd s/m^2 in *Mll5*-KO mice but was unchanged at lower stimulation intensities (Figure 1K). The amplitude of the positive b-wave, which originates from cone bipolar cells activated by cone photoreceptors, was also significantly decreased at higher stimulus intensities (2.1–3.3 log cd s/m^2) (Figure 1L). It is noted that *Mll5*-KO retinas showed more severe loss of both scotopic and photopic b-waves versus the loss of a-waves, indicating that MLL5 depletion may have more impact on the inner layers of the retinal bipolar cells. To determine whether visual decline in *Mll5*-KO retinas is caused by the Pde6brd1 mutation, which is a spontaneous lesion common among laboratory inbred mice arising from a murine viral insertion in exon seven of the *Pde6b* (phosphodiesterase 6b) gene (Chang et al., 2002), we performed DNA sequence analysis of both *Mll5*-WT and *Mll5*-KO retinas. Both retinas are confirmed to carry the wild type *Pde6b* alleles (data not shown). Therefore, MLL5 depletion disrupts both scotopic and photopic ERG.

The change of ERG response of *Mll5*-KO mouse promotes us to investigate whether these changes were because of disrupted retinal structure. It is of note that *Mll5*-KO mouse eyeball size is not changed

compared to *Mll5*-WT, although *Mll5*-deficient mouse exhibited systemic abnormalities (Zhou et al., 2018). Hematoxylin-and-eosin (H&E) staining of retinal sections from three-week-old *Mll5*-HET and *Mll5*-KO mice revealed normal architectures (Figure S2A). There was also no change of the outer plexiform (OPL) and inner plexiform (IPL), indicated by staining of glutamine synthetase (GS) and protein kinase C alpha (PKCα) which label Müller cells and rod bipolar cells, respectively (Figure S2B). *Mll5*-KO retinas contained all major retinal cell types with grossly similar cell numbers to that of *Mll5*-WT retinas (Figure S2C), suggesting that depletion of MLL5 does not affect normal differentiation of the developing retina. To examine whether MLL5 depletion alters photoreceptor development, we performed immunostaining of *Mll5*-WT and *Mll5*-KO photoreceptors. Notably, expression of Rho, which is essential for light sensing in rod photoreceptors, was significantly decreased (Figures S2D–S2F). We also examined cone photoreceptor cells by immunostaining with an antibody against green cone opsin (anti-Opn1mw) as well as with fluorescently labeled lectin peanut agglutinin (PNA), which recognizes the outer and inner segments of cone photoreceptors. We observed a lower density of both PNA staining and dorsal retina Opn1mw staining in *Mll5*-KO mice compared with *Mll5*-WT mice, although the localization patterns were similar. We then performed terminal deoxynucleotidyl transferase-mediated biotinylated UTP nick end labeling (TUNEL) staining to compare rates of apoptosis in *Mll5*-WT and *Mll5*-KO retinas from P21 mice. A significantly higher number of TUNEL-positive cells (~10-fold) were detected in retinas from *Mll5*-KO mice compared with those from *Mll5*-WT (Figures S2G and S2H). We then evaluated the number of photoreceptor nuclei in the outer nuclear layer (ONL). Compared with *Mll5*-WT retinas that contain 10–11 layers of photoreceptor nuclei in the ONL, *Mll5*-KO mice at the age of 6 weeks retained only eight to nine layers of photoreceptor nuclei (Figure S2I). Other layers of *Mll5*-KO retinas had normal cell numbers (data not shown). These data demonstrate that loss of MLL5 induces mild retinal degeneration, consistent with the ERG amplitude reductions, suggesting that MLL5 is important in photoreceptor maintenance.

Depletion of MLL5 impairs the expression of critical photoreceptor genes

Because MLL5 depletion did not change the retinal architecture, we then investigated whether the attenuated ERG is caused by defects on retinal gene expression. We examined genome-wide gene-expression profiles of *Mll5*-WT and *Mll5*-KO retinas using high-throughput RNA sequencing (RNA-seq). Two bioreplicates of RNA-seq were performed using *Mll5*-WT and *Mll5*-KO retinas at P18 (Figure 2A). A total of 133 genes were found to be dysregulated with at least 2-fold differential expression. In *Mll5*-KO retinas, 82 genes were downregulated and 51 genes were upregulated compared with *Mll5*-WT retinas. Functional annotation of the differentially expressed genes using gene ontology (GO) analysis (DAVID web tool) showed enrichment of processes related to visual perception, photoreceptor cell development, and photoreceptor maintenance among the downregulated genes, whereas the upregulated genes were enriched for processes related to cell cycle and cell proliferation (Figure 2B and Table S1). Notably, a number of differentially expressed genes between *Mll5*-KO and *Mll5*-WT retina are known to be mutated in inherited human retinal diseases or have been shown to be essential for retinal organization and vision function (Figure 2C). qPCR analysis confirmed a significant reduction in mRNA expression of photoreceptor-specific genes, such as *Rho*, *Opn1sw* (blue cone opsin), and *Opn1mw* in *Mll5*-KO retinas (Figure 2D), whereas the expression of cell-type specific genes from different retinal neuronal cell types did not significantly change, except for *Rlbp1* (Retinaldehyde-binding protein 1) (Figure S3A). Furthermore, MLL5 depletion did not affect the expression of well-known photoreceptor transcription factors, such as CRX, NRL (neural retina-specific leucine zipper), and Nr2e3 (nuclear receptor subfamily two group E member 3) (Figure S3B), and no significant changes were observed in the expression of core transcription factors and signaling proteins essential for progenitor cell maintenance (Figure S3C). These findings suggest that MLL5 promotes retinal maturation and maintenance through regulating genes essential for photoreceptor organization and function and not via induction of altered expression of key retinogenesis regulators.

MLL5 is required for CRX-mediated photoreceptor gene transactivation

To investigate whether MLL5 is directly involved in photoreceptor gene transcription, we examined the effect of MLL5 knockdown on *Rho* transcription using a *Rho* promoter-based luciferase assay. A region containing the human *Rho* (*HsRho*) distal and proximal promoters (positions −1500 to +10) driving a Firefly luciferase gene was cloned into the pGL3 vector and transfected into HEK293T cells together with an internal control plasmid expressing Renilla luciferase. In line with previous studies (Chen et al., 1997; Irie et al., 2015), the *HsRho* promoter was significantly activated when the transcription factor CRX was introduced, whereas introduction of MLL5 alone showed marginal transactivation of the *HsRho* promoter. However, we observed a significant decrease in *HsRho* promoter activity when endogenous MLL5 was depleted using

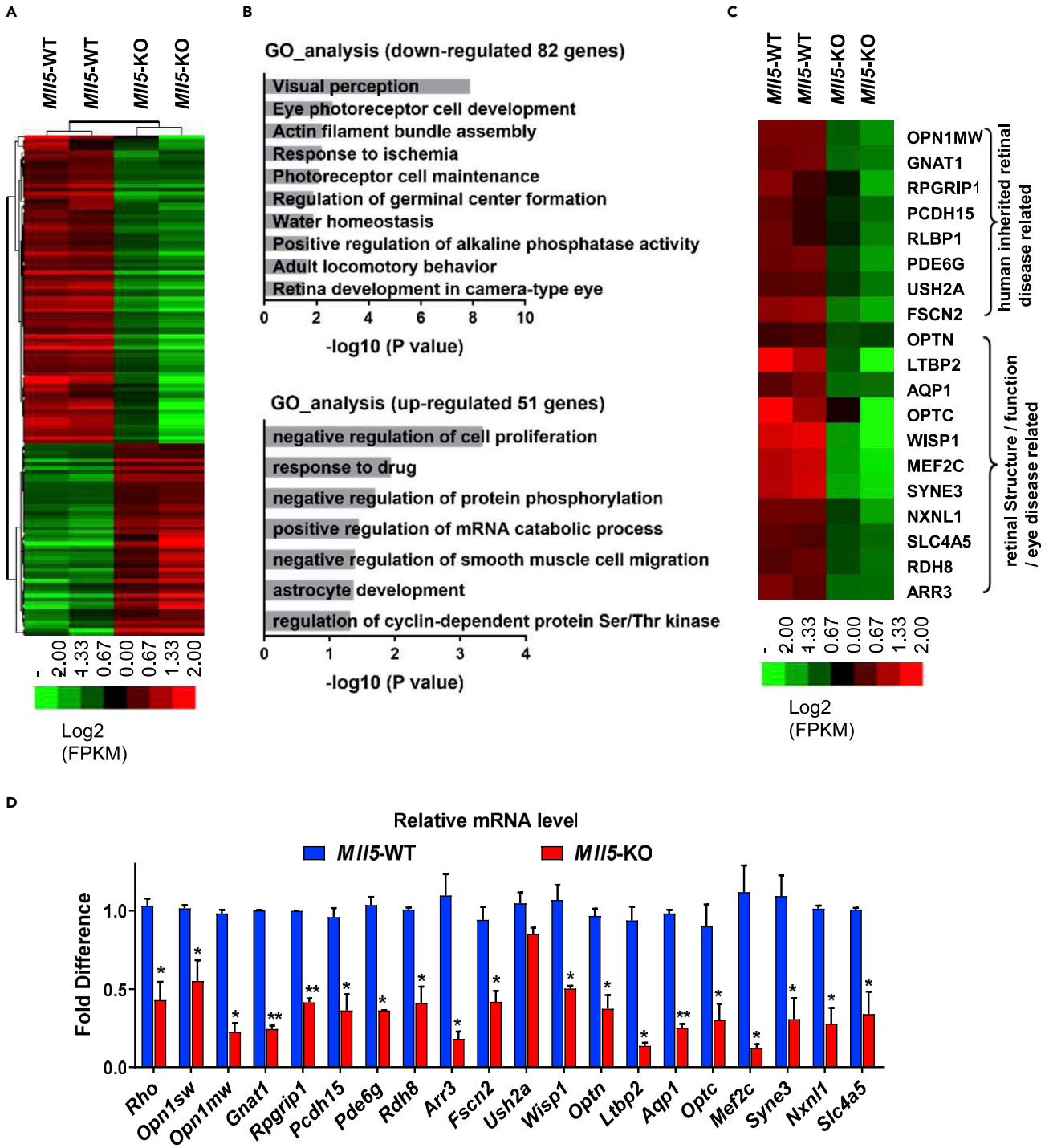

Figure 2. Gene expression analysis of *Mll5*-WT and *Mll5*-KO retinas

(A) RNA-seq heatmap showing expression patterns of 133 dysregulated genes in *Mll5*-KO retinas at P16. The expression values are Log2 (FPKM) values and are indicated with green or red colors representing lowest to highest expression levels.

(B) Gene ontology (GO) analysis of downregulated and upregulated genes in *Mll5*-KO retinas showing the top 10 enriched GO terms. The value of –log10 (p value) was calculated to reflect the significance of GO term enrichment.

(C) Heatmap depicts the Log2 (FPKM) values of *Mll5*-KO affected genes that are involved in human retinal disease, retina development, and visual functions.

(D) Bar chart showing the downregulation of selected photoreceptor genes and genes that were found dysregulated in RNA-seq analysis. qPCR analysis was performed using P16 *Mll5*-WT and *Mll5*-KO retinas and was normalized to the expression of *Tbp* (TATA binding protein) (n = 3). Error bars show the SEM (n = 5). *p < 0.05, **p < 0.01, ***p < 0.001, Student's t test.

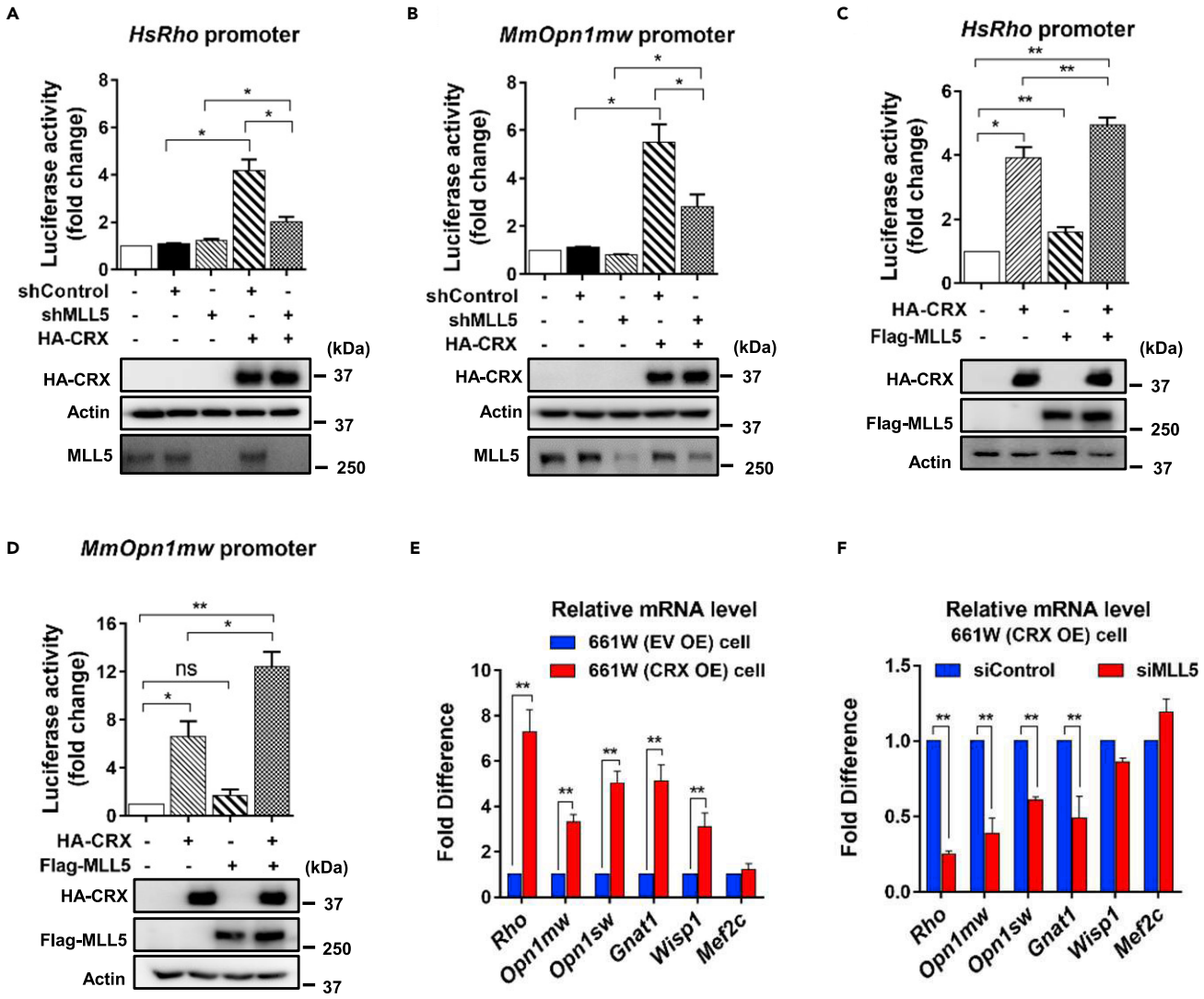

Figure 3. MLL5 is required for CRX-mediated photoreceptor gene transactivation

(A and B) Luciferase reporter assay to study the transactivation of *HsRho* and *MmOpn1mw* promoters in the absence of MLL5. HEK293T cells were transfected with control shRNA (shControl) or MLL5-shRNA (shMLL5) to knockdown endogenous MLL5 at 24 h before introducing CRX, *Opsin* promoter luciferase constructs, and Renilla luciferase. Dual-luciferase reporter assays were performed and the Firefly values were normalized to Renilla luciferase. Data are presented as ratios of the value for each combination to the value for the reporter plasmid transfected together with an empty vector. Overexpression of HA-CRX and endogenous MLL5 were determined by western blotting. Error bars represent SEM (n = 3).

(C and D) Luciferase reporter assay to study the transactivation of *Rho* and *Opn1mw* promoters by using MLL5 and CRX. As for panel (A and B), except that HEK293T cells were sequentially transfected with Flag-MLL5 and then HA-CRX together with Firefly luciferase constructs and Renilla luciferase. Overexpression of HA-CRX and Flag-MLL5 was determined by western blotting. Error bars represent SEM (n = 3).

(E) qPCR analysis showing upregulation of selected photoreceptor genes in 661W (CRX OE) cells compared with those in 661W (EV OE) cells (normalized to expression of Tbp). Error bars represent SEM (n = 3).

(F) qPCR analysis showing reduced expression of selected photoreceptor genes in 661W (CRX OE) cells following MLL5 knockdown with *Mll5* specific siRNA duplexes #1. Error bars represent SEM (n = 5). *p < 0.05, **p < 0.01, ***p < 0.001, Student's t test.

MLL5-shRNA (shMLL5) (Figure 3A). We performed similar assays on the murine *Opn1mw* (*MmOpn1mw*) promoter (positions −1441 to −14) and the *Opn1sw* (*MmOpn1sw*) promoter (positions −1450 to −11). A significant decrease in the transactivation of both promoters was also observed in the presence of shMLL5 (Figures 3B and S4A). Next, we examined if MLL5 and CRX synergistically regulate the expression of photoreceptor genes. Enhancement of *HsRho* transactivation was detected when exogenous MLL5 was co-transfected with CRX (Figure 3C); however, the effect was marginal, presumably owing to the preoccupancy of endogenous MLL5 saturating MLL5-binding sites. Similar results were obtained in the transactivation of

MmOpn1mw and *MmOpn1sw* promoters (Figures 3D and S4B). It is of note that these transient transfections of episomal luciferase may not contain appropriate chromatin (nucleosomal) structure and result in false-positive results. To exclude this possibility, we next investigated if MLL5 is required for photoreceptor gene transcription using 661W. The 661W photoreceptor cell line was derived from mouse retinal tumor and has been widely used as a model for studying macular degeneration (Tan et al., 2004). Previous studies found that 661W cells expressed the majority of markers of cone cell origin (Wheway et al., 2019). It could be multipotent and could be differentiated to a neuronal phenotype (Thompson et al., 2015). Transduction of 661W using lentivirus has been reported (Hamann et al., 2013; Zhou et al., 2021). We transduced HA-tagged CRX and an empty control vector into 661W cells with retroviral particles (Figures S5A–S5C), hereafter referred to as 661W (CRX OE) cells and 661W (EV OE) cells. Photoreceptor gene expression was then examined in both cells. Five out of six CRX-targeting genes (Hsiau et al., 2007; Tran et al., 2014), including *Rho*, *Opn1mw*, *Opn1sw*, *Gnat1*, and *Wisp1*, were prominently augmented in the presence of ectopically expressed CRX (Figure 3E). Notably, the expression of *Rho*, *Opn1mw*, *Opn1sw*, and *Gnat1* was significantly reduced when endogenous MLL5 was depleted using *Mll5* specific siRNA duplexes (Figure 3F). In contrast, the expression of *Mef2c* was not activated by CRX and was also not affected by MLL5 knockdown. These data suggest that MLL5 is essential for the transcription of a subset of photoreceptor genes. Therefore, the data indicates that MLL5 cooperates in the transactivation of *opsin* promoters induced by CRX.

MLL5 interacts with CRX via its CD4 domain

The importance of MLL5 in CRX-mediated photoreceptor gene transactivation led us to investigate whether MLL5 interacts with CRX directly. Thus, we conducted co-immunoprecipitation (co-IP) studies in retinal lysates from P18 *Mll5*-WT or *Mll5*-KO mice using anti-MLL5 or anti-CRX antibodies, which revealed an interaction between endogenous MLL5 and CRX (Figure 4A). To determine which region of MLL5 binds CRX, we expressed three truncated Flag-MLL5 mutants together with HA-CRX in HEK293T cells and performed co-IP using an anti-HA antibody. HA-CRX was shown to bind the central domain (CD) of MLL5, rather than the PHD/SET domain (PS) or the C-terminal domain (CT) (Figures 4B and 4C). A smaller fragment of the MLL5 CD domain (CD4) was then co-expressed with HA-CRX in HEK293T. As shown in Figure 4D, Flag-MLL5-CD4 maintained its ability to bind HA-CRX. In line with this, an MLL5 mutant construct lacking the CD4 region failed to interact with CRX, indicating that MLL5-CD4 is the key binding region for CRX (Figure 4E). We then examined whether the interaction between MLL5-CD4 and CRX is essential for CRX-mediated transactivation. We incubated 661W (CRX OE) cells with siMLL5 for 16 h to knockdown endogenous MLL5 and then ectopically introduced RNAi-resistant full-length MLL5 (MLL5-FL) or an RNAi-resistant CD4 domain deletion construct (MLL5-ΔCD4) using lentivirus particles. Noninfected 661W cells were eliminated by puromycin selection. MLL5 knockdown reduced *Rho* transcription in 661W (CRX OE) cells, which could be rescued by MLL5-FL overexpression; however, transcription could not be rescued using MLL5-ΔCD4 (Figure 4F). These data demonstrate that CRX binds the CD4 domain of MLL5, and this interaction is required for photoreceptor gene transactivation.

MLL5 and CRX co-occupy on *Rho* promoter

The critical role of MLL5 in CRX-mediated photoreceptor gene transactivation (Figure 3) and the physical interaction between MLL5 and CRX (Figure 4) raised the possibility that MLL5 is required for efficient or stable recruitment of CRX to photoreceptor gene promoters. A number of studies have shown that dysregulation of Rho underlies a spectrum of inherited human retinal disease; therefore, we focused our mechanistic studies on the regulation of the *Rho* gene. We performed qChIP (Quantitative ChIP) analysis on *Mll5*-WT and *Mll5*-KO mouse retinas using four primer pairs at intervals of approximately 400 bp, corresponding to different regions of the *Rho* promoter locus. Primer pairs spanning the 3′-untranslated region (3′UTR) of the *Rho* gene were used as internal control. Consistent with previous studies (Corbo et al., 2010; Peng and Chen, 2007), CRX was enriched on the *Rho* promoter in *Mll5*-WT retinas, especially at a region immediately upstream of the TSS (primer pair −219 ∼ +46) and ∼1.5 kb upstream of the TSS, albeit at relative lower levels (primer pair −684 ∼ −443, −1150 ∼ −814 and −1500 ∼ −1311). Notably, CRX occupation on the *Rho* promoter decreased more than 2-fold in *Mll5*-KO retinas, indicating that MLL5 enhances the association of CRX with the *Rho* promoter (Figure 5A). A requirement for CRX in the recruitment of CBP to *Opsin* promoters has been reported previously in murine retina and Y79 retinoblastoma cells (Peng and Chen, 2007). CBP has intrinsic histone acetyltransferase activity targeted to histones H2A, H2B, H3, and H4 (Peterson and Laniel, 2004). Consistent with these findings, MLL5 depletion also reduced CBP accumulation at the *Rho* promoter. H3Ac and RNA polymerase II recruitment on the *Rho* promoter in *Mll5*-KO retinal tissue was reduced by more than 2-fold compared with *Mll5*-WT retinal tissue

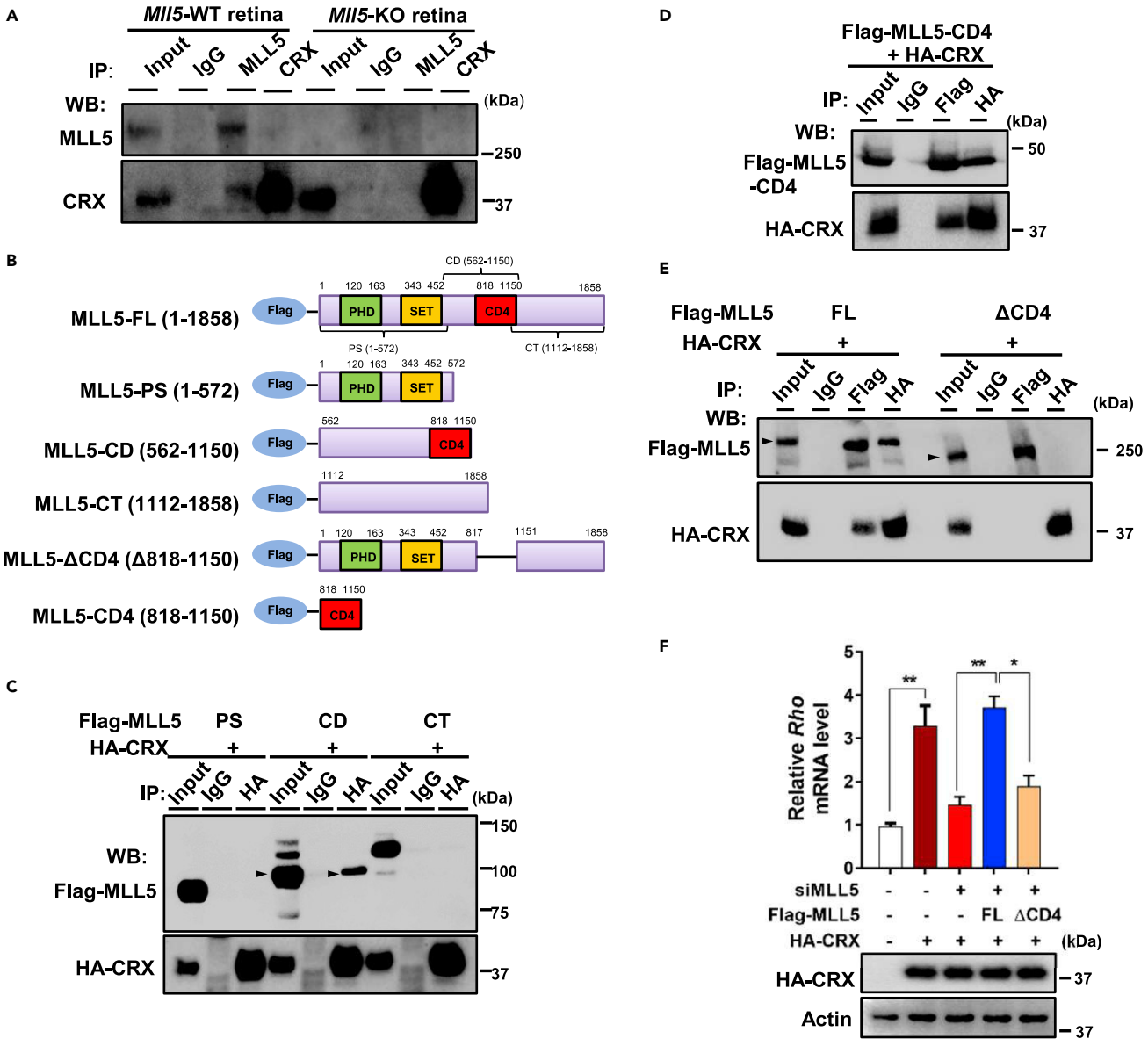

Figure 4. MLL5 interacts with CRX via its CD4 domain

(A) Interaction between endogenous MLL5 and CRX. Equivalent amounts of retinal lysates from *Mll5*-WT or *Mll5*-KO mice were immunoprecipitated with anti-MLL5 antibody, anti-CRX or normal rabbit IgG, followed by western blotting detection.

(B) Schematic representation of MLL5 truncated mutants. PS, PHD/SET domain; CD, central domain; CT, C-terminal domain. ΔCT4, deleted CT4 domain.

(C) MLL5 central domain (MLL5-CD) binding to CRX. HEK293T cells expressing HA-CRX together with Flag-MLL5-PS, Flag-MLL5-CD, or Flag-MLL5-CT were subjected to immunoprecipitation with the indicated antibodies followed by western blotting detection.

(D) Interaction between MLL5-CD4 and CRX. HEK293T cells expressing HA-CRX and Flag-MLL5-CD4 were immunoprecipitated with anti-HA antibodies and detected by anti-Flag and anti-HA antibodies.

(E) Depletion of MLL5 CD4 compromises MLL5 interaction with CRX. HEK293T cells expressing HA-CRX along with Flag-MLL5-FL or Flag-MLL5-ΔCD4 were immunoprecipitated with anti-HA and anti-Flag antibodies followed by western blotting detection.

(F) MLL5-ΔCD4 was less potent than MLL5-WT at rescuing transcription of *Rho*. qPCR analysis of *Rho* transcript in 661W (CRX OE) cells transfected with MLL5-siRNA (siMLL5) followed by transduction with the indicated lentivirus. Rho expression was normalized to the expression of Tbp. Error bars represent SEM (n = 3), **p < 0.01, Student's t test. Results in (A–F) are representative of at least three experimental repeats.

(Figure 5A). As previously reported (Peng and Chen, 2007), CRX, CBP, and H3Ac did not accumulate at the 3'UTR of the *Rho* gene. We also detected CRX, CBP, and H3Ac recruitment on the promoter of *Collagenase* gene. *Collagenase* gene is a non-photoreceptor-specific gene, and previous study has shown that it cannot

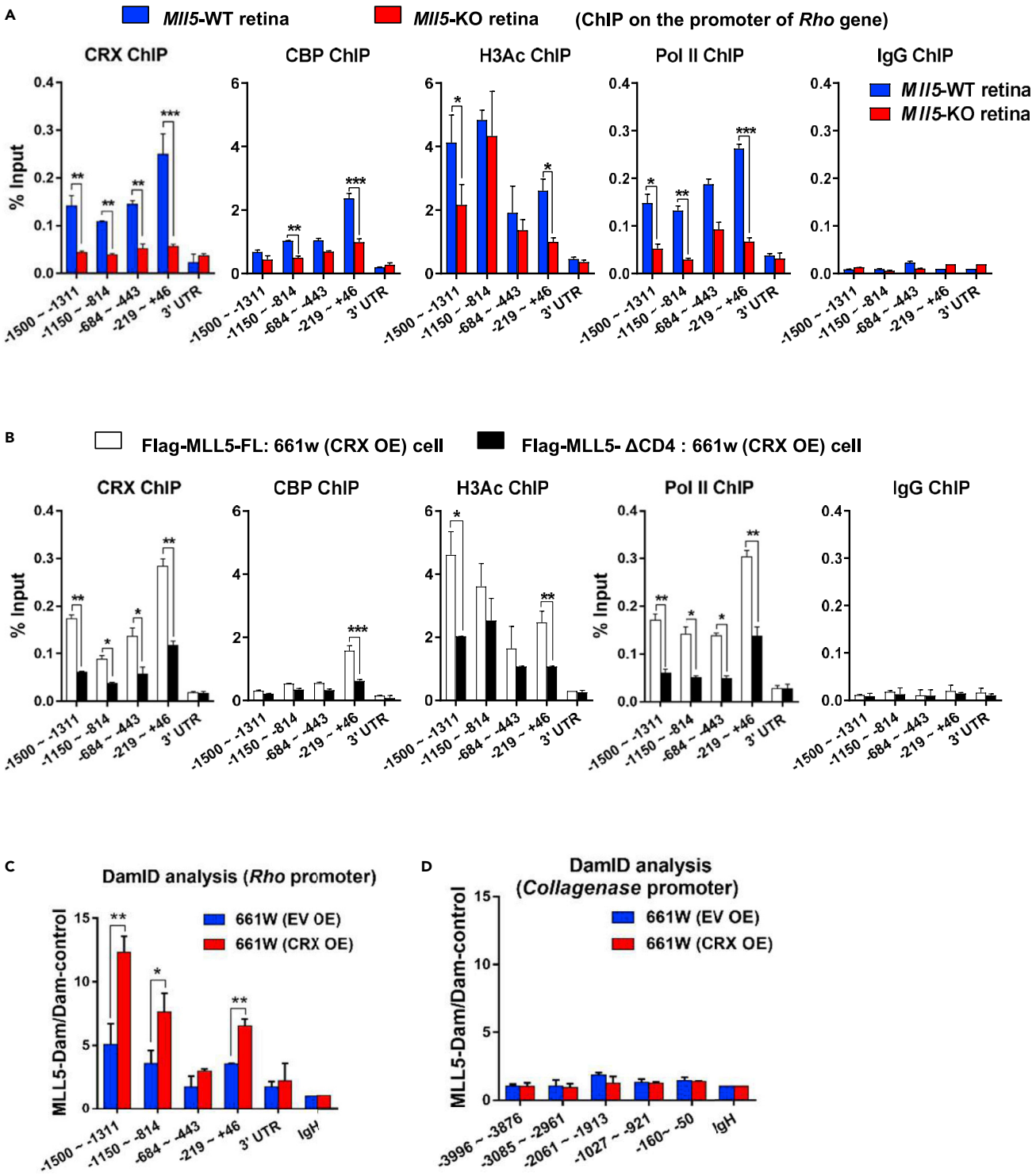

Figure 5. MLL5 and CRX co-occupy the *Rho* promoter

(A) MLL5 depletion leads to reduced binding of CRX, CBP, and Pol II (RNA Polymerase II), as well as decreased H3Ac (H3 acetylation) at the *Rho* promoter. qChIP (Quantitative ChIP) analysis using P18 *Mll5*-WT and *Mll5*-KO retinas with antibodies against CRX, CBP, Pol II, acetylated H3 (H3Ac), or normal rabbit IgG. Immunoprecipitated DNA fragments were analyzed by qPCR for the promoter region and 3′ UTR regions of *Rho* gene. All data shown are representative qChIP and presented as % of input chromatin. Error bar shows mean SEM (n = 3 from six retinas). **p < 0.01, ***p < 0.001, Student's t test.

Figure 5. *Continued*

(B) Recruitment of CRX, CBP, Pol II, and acetylated H3 at the *Rho* promoter are decreased in 661W (CRX OE) cells when the ΔCD4 domain of MLL5 was deleted. 661W (CRX OE) cells, depleted of endogenous MLL5 using siRNA, were further transduced with MLL5-WT or MLL5-ΔCD4 by lentivirus. qChIP analysis was performed with antibodies against CRX, CBP, Pol II, H3Ac, or normal rabbit IgG. Immunoprecipitated DNA fragments were analyzed by qPCR for the region of the *Rho* promoter and 3'UTR. Representative qChIP data of at least three experimental repeats are shown and presented as % of input chromatin. Error bar represents SEM (n = 3). **p < 0.01. ***p < 0.001, Student's t test.

(C and D) CRX enhances the recruitment of MLL5 at the *Rho* promoter but not at the *Collagenase* promoter. 661W (EV OE) cells and 661W (CRX OE) cells were transduced with MLL5-Dam or Dam-control by lentivirus followed by G418 selection to remove noninfected cells. Genomic DNA was then harvested and subjected to a DamID protocol, followed by qPCR using primers in the proximity to the promoter regions of *Rho*, 3'UTR, within the enhancer of immunoglobulin heavy chain (IgH), or the promoter regions of Collagenase as negative control. Data are presented as ratios of the MLL5-Dam qPCR signal to the Dam-only signal. Representative results of at least three experimental repeats are shown. Error bar represents SEM (n = 3), *p < 0.05. **p < 0.01, Student's t test.

be transactivated by CRX (Chen et al., 1997). We found that there was no enrichment of CRX, CBP, and H3Ac on the promoter of *Collagenase* gene in *Mll5*-WT and *Mll5*-KO retinas (Figure S6).

To determine whether decreased recruitment of CRX/CBP is a consequence of the attenuated interaction between MLL5 and CRX, we depleted endogenous MLL5 and then introduced RNAi-resistant MLL5-FL or MLL5-ΔCD4 into 661W (CRX OE) cells. Consistent with our qChIP results in *Mll5*-WT retinas, the *Rho* promoter displayed CRX accumulation, CBP binding, H3 acetylation, and RNA polymerase II recruitment in 661W cells expressing MLL5-FL, although these effects were significantly decreased in MLL5-ΔCD4 expressing 661W cells (Figure 5B). Collectively, these data demonstrate that MLL5 play a role in the recruitment or stabilization of CRX/CBP to the *Rho* promoter, which is dependent on the direct interaction between CRX and MLL5.

Next, we asked whether CRX could alter MLL5 recruitment to chromatin. A lack of ChIP-grade antibodies capable of detecting mouse MLL5 meant that we could not investigate MLL5 occupancy on the *Rho* promoter *in vivo*. As an alternative, we employed DNA adenine methyltransferase identification (DamID), a well-established assay for measuring protein-DNA interactions (Vogel et al., 2007), which has previously been used to determine the genomic distribution of MLL5 in C2C12 cells (Ali et al., 2013). Briefly, MLL5 was fused to the N-terminal of the *Escherichia coli's* DNA adenosine methyltransferase (Dam) and transduced into control or 661W (CRX OE) cells. Genomic DNA was then isolated and processed to amplify methylated DNA, corresponding to particular regions targeted by MLL5. Cells infected with Dam-control lentivirus served as a control for background DNA methylation. As expected, only a negligible recruitment of MLL5-Dam was observed at the silent immunoglobulin heavy chain enhancer (Buas et al., 2010), which was used to normalize the data. 661W (EV OE) cells expressing MLL5-Dam gave rise to more than 3-fold relative increase in methylation in the *Rho* promoter but not in the vicinity of the *Rho* 3'UTR (Figure 5C). Methylation at the *Rho* distal and proximal promoter regions was further enhanced in 661W (CRX OE) cells transduced with MLL5-Dam (Figure 5C). MLL5 binding on the promoter of *Collagenase* was also examined by Dam-ID. As expected, 661W cells infected with MLL5-Dam did not generate significantly increased relative methylation on the promoter of *Collagenase* gene (Figure 5D). These data indicate that MLL5 associates specifically with the *Rho* promoter, primarily at ~1.5 kb upstream of the TSS, and this binding is further enhanced by CRX. Collectively, these data suggest that MLL5 and CRX are co-recruited to the *Rho* promoter interdependently.

MLL5 is critical for the methylation of histone H3K4 and H3K79 on the *Rho* promoter

Since it has been suggested that MLL5 might affect H3K4 methylation indirectly by affecting the expression of LSD1 (lysine-specific histone demethylase 1), and SET7/9 in C2C12 murine myoblast cells (Sebastian et al., 2009). We asked whether MLL5 depletion affects histone methylations. Immunoblot analysis revealed similar levels of genome-wide H3K4me1, H3K4me2, H3K9me2, and H3K36me2 in *Mll5*-WT and *Mll5*-KO retinas (Figure 6A), whereas global levels of H3K4me3 and H3K79me2 were reduced in *Mll5*-KO retinas at P18 and in MLL5 knockdown 661W cells. This is different from *Mll1* conditionally knocked out retinas which displayed similar levels of H3K4me3 as in CreNeg control retinas (Brightman et al., 2018). We then detected histone methylations on *Rho* promoter by qChIP analysis. We found an enrichment of H3K4me2/3 on the *Rho* promoter in *Mll5*-WT retinas, corresponding to its active expression, as well as in the gene coding regions, consistent with a genome-wide analysis of H3K4 methylation in retina (Popova et al., 2012). Notably, H3K4me2/3 accumulation on *Rho* promoter was reduced by more than 2-fold in *Mll5*-KO retinas, which may contribute to *Rho* repression in *Mll5*-KO retinas; however, MLL5 depletion did not affect the H3K4me2/3 level on *Rho* gene 3' UTR (Figure 6B). H3K79me2 was also detected on *Rho* promoter, which was reduced in *Mll5*-KO retinas (Figure 6B). We also detected H3K4/K79 methylation on *Collagenase* gene in *Mll5*-WT and *Mll5*-KO retinas, and found that there was no

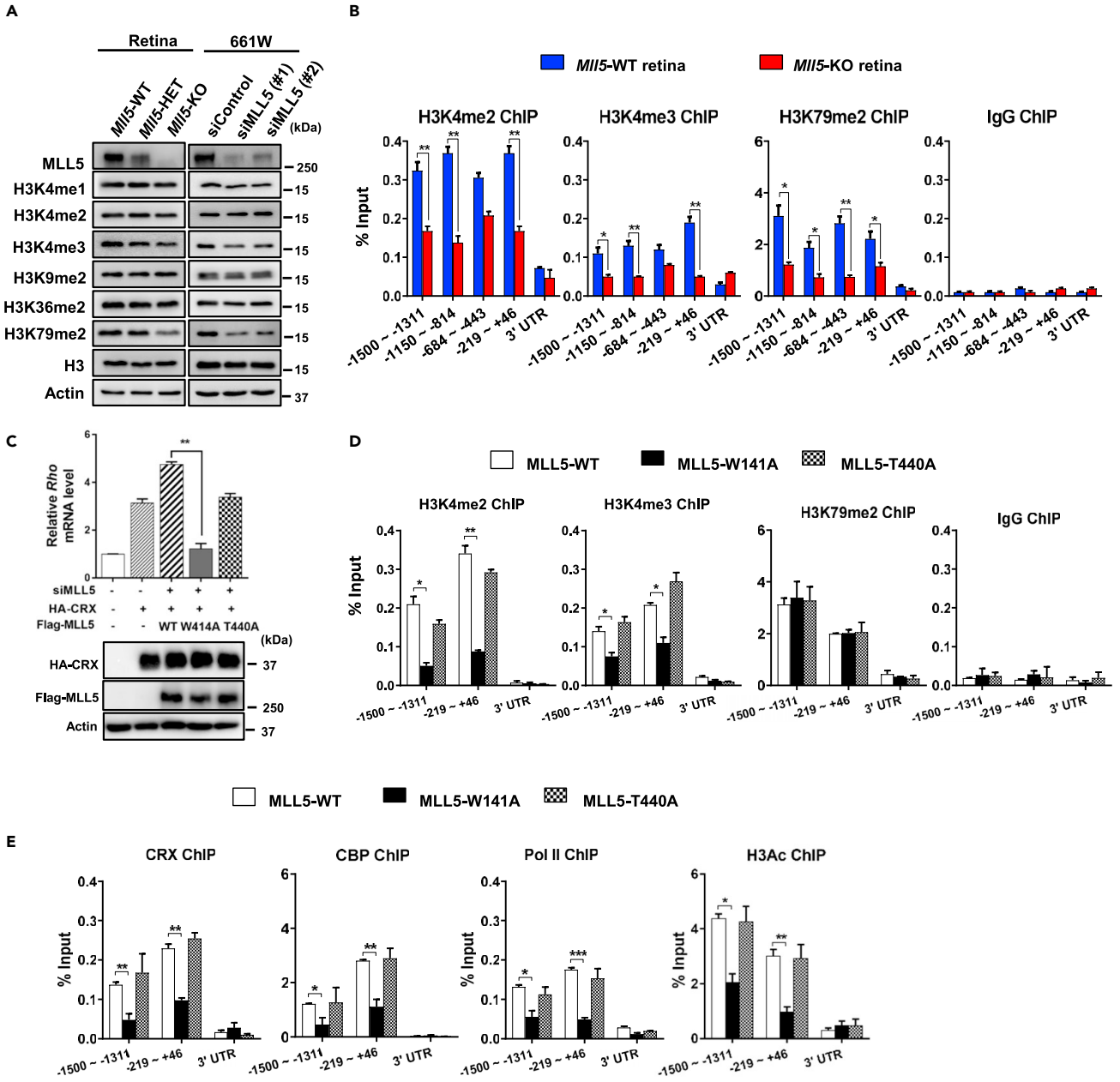

Figure 6. MLL5 is critical for the methylation of histone H3K4 and H3K79 on the *Rho* promoter

(A) Representative western blotting of at least three experimental repeats shows reduced global H3K4me3 and H3K79me2 levels in *Mll5*-KO retinas. Equivalent amounts of protein (5 μg) were loaded for each panel.

(B) MLL5 depletion leads to decreased H3K4me2/3 and H3K79me2 levels at the *Rho* promoter. qChIP (Quantitative ChIP) analysis using P18 *Mll5*-WT and *Mll5*-KO retinas with antibodies against H3K4me2, H3K4me3, H3K79me2, or normal rabbit IgG. Immunoprecipitated DNA fragments were analyzed by qPCR for the promoter region and gene coding region of *Rho* gene. All data shown are representative qChIP and presented as % of input chromatin. Error bar shows mean SEM (n = 3 from six retinas). **p < 0.01, ***p < 0.001, Student's t test.

(C) qPCR analysis shows that the MLL5-W141A mutant failed to rescue *Rho* expression in MLL5-KD 661W (CRX OE) cells. 661W (CRX OE) cells were transfected with MLL5-siRNA (siMLL5) for 16 h and then infected with lentivirus particles expressing RNAi-resistant Flag-MLL5 or RNAi-resistant domain mutant MLL5 constructs. Noninfected cells were eliminated by puromycin selection. Overexpression of MLL5 and CRX was determined by western blotting. Error bars represent SEM (n = 3).

(D and E) qChIP analysis shows that MLL5 PHD finger mutation did not affect the recruitment of H3K79me2 but caused decreased recruitment of H3K4me2/3, CRX, CBP, Pol II, and H3Ac to the *Rho* promoter. 661W (CRX OE) cells were transfected with siMLL5 and then transduced with MLL5-WT, -W141A, or –T440A

Figure 6. *Continued*

by lentivirus. qChIP analysis was performed with antibodies against H3K4me2, H3K4me3, H3K79me2, CRX, CBP, Pol II, H3Ac, or normal rabbit IgG. Immunoprecipitated DNA fragments were analyzed by qPCR for the promoter and gene coding regions of *Rho* gene. All qChIP data shown in Figure 6 are representative qChIP results from at least three experimental repeats and presented as % of input chromatin. Error bars represent SEM (n = 3 from six retinas). *p < 0.05, **p < 0.01, ***p < 0.001, Student's t test.

H3K4me3 and H3K79me2 on *Collagenase* gene (Figure S6). High H3K4/K79 methylation has been associated with preengaged basal transcription machinery (Guccione et al., 2006). We found that RNA polymerase II bound on *Rho* gene but not *Collagenase* gene in retinas, and this binding was reduced in *Mll5*-KO retinas at P18 (Figures 5A and S6). Collectively, these data suggest MLL5 depletion reduced methylation of H3K4 and H3K79 on *Rho* gene, which may contribute to reduced RNA polymerase II bounding on *Rho* gene and *Rho* gene repression in *Mll5*-KO retinas.

The MLL5 PHD finger is critical for CRX recruitment to *Rho* promoter

It has been demonstrated that MLL5 and RNA polymerase II co-occupy promoters that display H3K4me3, suggesting that MLL5 may have the capacity to read H3K4me3 modification, and recognition of the H3K4me3 can facilitate the recruitment of MLL5 to active transcription chromatin regions. Further studies indicated that MLL5 binds strongly and specifically to histone H3K4me3 through its PHD finger, and substitution of W141 with an alanine completely abolished the MLL5 PHD finger and H3K4me3 interaction (Ali et al., 2013; Lemak et al., 2013; Zhang et al., 2017). We then examined whether the MLL5 PHD finger has a role in *Rho* transactivation. We first dissected to find whether mutations in the PHD finger could alter *Rho* transactivation. We depleted endogenous MLL5 and then transduced exogenous RNAi-resistant wild-type-MLL5 (MLL5-WT) or MLL5-W141A mutants into 661W (CRX OE) cells. Notably, MLL5-WT protein restored *Rho* transcription, whereas the MLL5-W141A mutant, which disrupts MLL5 binding to H3K4me2/3, failed to do so (Figure 6C). T440 is a conserved site of O-GlcNAcylation in two short forms of MLL5 (Ding et al., 2015; Nin et al., 2015). *Rho* transactivation was not affected by transduction of the MLL5-T440A mutant, indicating that glycosylation is not involved in this interaction (Figure 6C). Taken together, our results suggest that the MLL5 PHD finger is essential for *Rho* transactivation.

To assess how the PHD finger functions on *Rho* gene transactivation, we sought to determine whether MLL5 recruitment to chromatin through PHD finger is required for the recruitment of CRX-CBP to activate Rho transcription. We first checked whether the MLL5 PHD finger is required for H3K4me3 and H3K79me2 on the *Rho* promoter. qChIP analysis in endogenous MLL5-depleted 661W (CRX OE) cells revealed high levels of H3K4me2/3 at the *Rho* promoter in the presence of exogenous MLL5-WT, which was reduced by more than 2-fold when exogenous MLL5-W141A mutant was transduced. Importantly, PHD domain mutation did not affect the H3K79me2 at the *Rho* promoter. Expression of the glycosylation site mutant exogenous MLL5-T440A did not alter H3K4me2/3 and H3K79me2 at the *Rho* promoter (Figure 6D). We next detected whether PHD finger mutation affects CRX-CBP binding to the *Rho* promoter by qChIP. As expected, CRX and CBP were recruited to the *Rho* promoter in the presence of exogenous MLL5-WT. However, enrichment of both molecules was reduced by more than 2-fold in the presence of MLL5-W141A mutant versus MLL5-WT. Reduced RNA polymerase II binding on the *Rho* promoter was also detected in the cells expressing MLL5-W141A mutant, but not in MLL5-T440A-expressing cells (Figure 6E). Collectively, these results demonstrate that MLL5 directly influences CRX-CBP recruitment to the *Rho* promoter, possibly through recognition of H3K4me2/3 by its PHD finger.

DISCUSSION

Histone modifications and transcription factors are important components of transcriptional regulation. Despite increasing numbers of studies demonstrating that H3K4 methylation and CRX are both involved in photoreceptor gene transactivation and maturation, whether H3K4 methylation links to transcription factor recruitment is undetermined. Our data indicate that an intact PHD finger is essential for the MLL5 function on photoreceptor gene transcription, with mutations of the PHD finger leading to compromised CRX-CBP assembly. In *Mll5*-KO retinas, loss of MLL5 leads to decreased H3K4/K79 methylation and impaired CRX-CBP occupancy on photoreceptor gene promoters, reducing histone acetylation and photoreceptor gene transcription, which results in impaired retinal function (Figure 7A). Moreover, we observed that MLL5 interacts with CRX via its CD4 domain, and the interdependent recruitment of MLL5 and CRX to the *Rho* promoter is essential for *Rho* activation. The MLL5 PHD domain may anchor MLL5 to chromatin through recognition of H3K4me2/3, which is a prerequisite for CRX recruitment to chromatin. CRX then assembles CBP, which catalyzes histone H3 acetylation, facilitating RNA polymerase II transcription of *Rho*

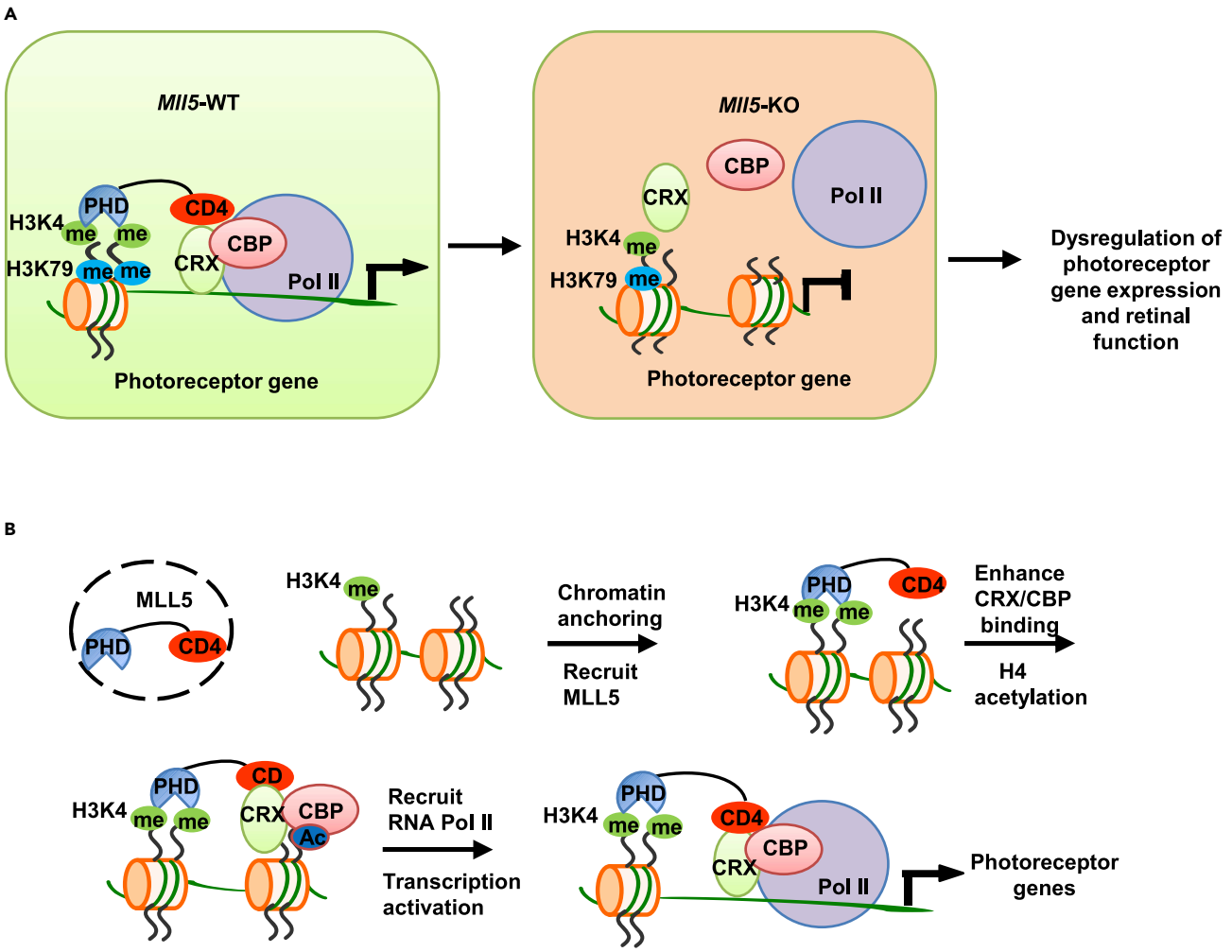

Figure 7. Model for the action of MLL5 on photoreceptor gene transcription activation

(A) MLL5 is required for photoreceptor gene expression and normal eye vision, as well as retinal maintenance. In *Mll5*-KO retinas, both CRX and CBP expressions are not affected. However, MLL5 depletion leads to reduced methylation of H3K4/K79, and decreased binding of CRX at photoreceptor gene promoters, which subsequently causes loss of HAT and Pol II binding, resulting in decrease of photoreceptor gene expression and abnormal retinal function. me, H3K4me3; Ac, histone H3 acetylation.

(B) In photoreceptor cells, H3K4 methylation marks photoreceptor specific genes. MLL5 recognises H3K4me2/3 via its PHD domain, which subsequently results in increased H3K4me3 level at promoters of photoreceptor genes. MLL5 also recruits CRX through its CD4 domain, which in turn enhances the recruitment of MLL5 to chromatin. CRX subsequently recruits CBP and activates the transcription of photoreceptor genes such as *Rho*, *Opn1mw*, and *Opn1sw*.

(Figure 7B). Hence, our study suggests that MLL5 acts as a cofactor for CRX to generate a permissive chromatin state for photoreceptor gene transcription and provides a new perspective on how photoreceptor-specific gene expression is established and maintained in the retina.

MLL5's role in coupling CRX and CBP with H3K4 methylation adds another layer of complexity to the spatiotemporal regulation of photoreceptor genes. Chromatin remodeling complexes and HAT-containing coactivators have been implicated in photoreceptor gene transcriptional activation, in concert with CRX (Hennig et al., 2008; Swaroop et al., 2010). Recent studies revealed that *Rho* activation is accompanied by *de novo* accumulation of H3K4me2/3, observed as early as P2 (Popova et al., 2012; Swaroop et al., 2010; Ueno et al., 2016). Notably, during mouse photoreceptor development, expression of CRX and CBP is present from the embryonic stage, whereas binding to the *Rho* promoter is only detected after P2 (Peng and Chen, 2007), suggesting that H3K4 methylation coincides with the establishment of the key basal transcription machinery required for *Rho* transcription. However, CRX itself is incapable of H3K4me2/3 recognition and requires assistance from MLL5, evidenced

by reduced CRX recruitment in the absence of MLL5 (Figure 5A). Further investigations into the co-occupancy of MLL5 and CRX and the co-occupancy of MLL5 and H3K4me2/3 on photoreceptor gene promoters using sequential ChIP analysis would be valuable once ChIP-grade anti-MLL5 antibodies become available.

To examine the spatial expression pattern of MLL5 in the murine retina, we performed ISH with an *Mll5* antisense probe. We also tried immunolocalization of MLL5 with two in-house generated and several commercially available anti-MLL5 antibodies. However, despite that they are suitable for Western blotting and immunofluorescent staining in cell lines, none of them were suitable for retinal cryostat sections and paraffin sections because of high background and poor specificity. It would be interesting to dissect the spatial and temporal expression of MLL5 during retinal development if antibodies for immunohistochemistry of retinal sections are available.

Previous studies have involved MLL5 in gene transcription regulation, although the underlying mechanism remains elusive. A study by Sebastian et al. showed that MLL5 negatively regulated *CCNA2* gene expression by binding to its proximal promoter in C2C12 cells (Sebastian et al., 2009). Another study on HsMLL5α, one of MLL5 isoforms, demonstrated that HsMLL5α is recruited to E2F1-responsive promoters by HCF1 in HEK293T and HeLa cells, resulting in activation of E2F1 target genes, such as *CCNA2*, *CDC2*, and *CDC6* (Zhou et al., 2013). Interestingly, both studies reported decreased H3K4me2/3 on *CCNA2* promoter but opposite regulation of *CCNA2* gene expression. We observed that MLL5 depletion reduced H3K4 methylation on the *Rho* promoter, whereas the underlying mechanism is still unclear. These data indicate that MLL5 may regulate gene transcription directly or indirectly in a cell-type/context-dependent manner (Zhang et al., 2017).

A compelling aspect of this study is that MLL5 appears to be a reader of H3K4me on Rho gene which is required for the recruitment of CRX-CBP and Histone acetylation. Intriguingly, putative MLL5 orthologues, including Up-SET, SET3/4, and SETD5 have been reported, as part of a histone deacetylase-containing complex that is recruited to transcribed genes to restrict histone acetylation and prevent inappropriate gene expression (Zhang et al., 2017); however, it is unclear how these orthologues are recruited to chromatin. Our results suggest that MLL5 potentially modulates photoreceptor-specific histone acetylation in a transcription factor-dependent manner through facilitating the recruitment of histone acetyltransferase instead of histone deacetylase. An earlier study also showed a similar gene activation regulation mechanism where Pax6-mediated recruitment of histone methyltransferases to lens gene chromatin contributes to the binding of histone acetyltransferase (HAT) p300 and the generation of enhancer-specific patterns of core histone modifications (Sun et al., 2016). Our data also demonstrate that H3K79 methylation is reduced in the absence of MLL5 in retinal cells.

In vitro studies have shown that Dot1L is the only known methyltransferase capable of H3K79 methylation (Feng et al., 2002), although there is evidence that another enzyme, RE-IIBP, can methylate H3K79 as well (Woo Park et al., 2015). However, we did not detect any interaction between MLL5 and DOT1L. The expression of DOT1L was also not affected in *Mll5*-KO retinas (data not shown). Further investigations into the recruitment of DOT1L or RE-IIBP on photoreceptor gene promoters may help explain why Rho promoter has lower H3K79me2 in *Mll5*-KO retinas.

A previous study characterizing the functions of the SET1/MLL family in the context of planarian regeneration demonstrated that *Smed-set1*, *-mll1/2*, *-trr-1*, and *-mll5-2*, which are clustered with vertebrate *SET1*, *Mll1/2*, *Mll3/4*, and *Mll5*, respectively, are required for visible photoreceptor regeneration (Hubert et al., 2013). Recent studies demonstrated that MLL1 plays an essential role in the neural development of zebrafish (Huang et al., 2015) and is indispensable for murine retinal neurogenesis and function development, although mechanistic study did not show gross H3K4 methylation change in *Mll1* depleted retinas (Brightman et al., 2018). Thus, it would be informative to study whether additional MLL family members play a role in the H3K4 methylation during retinal development.

Moreover, we found that MLL5 deficiency induced considerable increase of photoreceptor death, in concert with photoreceptor loss, although we could not determine from when did this start because of perinatal lethality of *Mll5-KO* mouse. *MLL5* gene transcript was detected in both the inner and outer retinas, and *Mll5*-KO retinas showed more severe loss of both scotopic and photopic b-waves versus the loss of a-waves. This suggests that MLL5 may not only function in photoreceptor cells in the ONL but also in the inner nuclear layer, such as bipolar cells and Müller cells. However, MLL5 depletion only affected the cell number of photoreceptor cell layers but not other neural layers and glial cells. The expression and localization of protein kinase C alpha (PKCα) which labels rod bipolar cells also showed normal expression. It is thus largely undetermined whether MLL5 also affects

retinal functions through regulation of bipolar cells. Interestingly, *MLL5* gene transcript was also detected in Müller cells. Although MLL5 depletion did not significantly reduce the expression of *Glu1* (Glutamine synthetase gene), the expression of *Rlbp1* was decreased in *Mll5*-KO retina. *Rlbp1 gene* is a key component of the retinal visual cycle in Müller cells that helps cone cells to function in high light intensities (Xue et al., 2015). It would be valuable to determine whether MLL5 also contributes to cone-driven vision and light responses through regulation of *Rlbp1*. Further discovery of MLL5 functions in other retinal neuronal cell types and in retinal degeneration would greatly advance our knowledge of MLL family members-mediated retinal development and maintenance.

Because mutations of Crx and Rho have been associated with human retinal disease, MLL5's interaction with CRX and its role in Rho regulation suggest that MLL5 depletion may also contribute to retinal disease pathogenesis. Further exploration of how an epigenetic regulator such as MLL5 and DOT1L take part in retinal development and maintenance will further our understanding on the fundamental mechanism of retinogenesis and clarify the role of epigenetic deregulation in retinal disease progression.

Limitations of the study

In this study, we showed MLL5 is required for photoreceptor gene transactivation. MLL5 expression was detected in both the inner and outer retinas, suggesting it functions not only in photoreceptors but also in other cell types. However, the *Mll5*-KO retina showed normal architecture. The expression of other cell-type specific genes from different retinal neuronal cell types also did not significantly change in the absence of MLL5, except for *Rlbp1*, an essential gene of Müller cells, which suggests that MLL5 may also have function in Müller cells. Further study will be required to better characterize MLL5 function in the inner nuclear layer.

STAR★METHODS

Detailed methods are provided in the online version of this paper and include the following:

- KEY RESOURCES TABLE
- RESOURCE AVAILABILITY
  - Lead contact
  - Materials availability
  - Data and code availability
- EXPERIMENTAL MODEL AND SUBJECT DETAILS
  - Mice
- METHOD DETAILS
  - Cell culture
  - siRNA transfection and plasmid constructions
  - RNA extraction, cDNA synthesis, and quantitative PCR (qPCR)
  - Immunoprecipitation (IP) and Western blotting
  - Histology and immunohistochemistry
  - Mouse retina *in situ* hybridization
  - Focal electroretinogram (fERG)
  - RNA-seq
  - Virus production and transduction
  - Dual-luciferase assay
  - Chromatin immunoprecipitation (ChIP) analysis
  - DamID assay
- QUANTIFICATION AND STATISTICAL ANALYSIS

SUPPLEMENTAL INFORMATION

Supplemental information can be found online at https://doi.org/10.1016/j.isci.2022.104058.

ACKNOWLEDGMENTS

We thank Dr. Al-Ubaidi for sharing 661W cell lines and Dr. Bas van Steensel for sharing DamID plasmids. We thank Dr. Md Zakir Hossain and his team in Transgenic & Gene Targeting Facility of CSI for recovery of live Mll5-HET mouse from cryopreserved sperms. We also thank the animal facility at National University of Singapore for supporting this project. We thank K. McLaughlin of Insight Editing London and Dawn Sijin Nin for critical review of the manuscript. This work is supported by Academic Research Fund Tier 1 grant

(R-183-000-405-114), Academic Research Fund Tier 2 grant (R-183-000-415-112), and the National Natural Science Foundation of China [81970838, 82125007, 81800857], Beijing Natural Science Foundation (Z200014), National Key R&D Program of China [2017YFA0105300].

AUTHOR CONTRIBUTIONS

X-M.Z., L-W.D., and Z-B.J. designed the research. X-M.Z., B-W.Z., L.X., H.W., A.S., P-P.Z., M.D., X-Y.W., W-J.X., and Y.Z. performed the research. X-M.Z., B-W.Z., L.X., and H.W., analyzed the data. X-M.Z. and L-W.D. wrote the manuscript.

DECLARATION OF INTERESTS

The authors declare no competing interests.

Received: August 23, 2021
Revised: December 11, 2021
Accepted: March 7, 2022
Published: April 15, 2022

REFERENCES

Ali, M., Rincón-Arano, H., Zhao, W., Rothbart, S.B., Tong, Q., Parkhurst, S.M., Strahl, B.D., Deng, L.-W., Groudine, M., and Kutateladze, T.G. (2013). Molecular basis for chromatin binding and regulation of MLL5. Proc. Natl. Acad. Sci. *110*, 11296–11301.

Bernt, K.M., Zhu, N., Sinha, A.U., Vempati, S., Faber, J., Krivtsov, A.V., Feng, Z., Punt, N., Daigle, A., Bullinger, L., et al. (2011). MLL-rearranged leukemia is dependent on aberrant H3K79 methylation by DOT1L. Cancer Cell *20*, 66–78. https://doi.org/10.1016/j.ccr.2011.06.010.

Brightman, D.S., Grant, R.L., Ruzycki, P.A., Suzuki, R., Hennig, A.K., and Chen, S. (2018). MLL1 is essential for retinal neurogenesis and horizontal inner neuron integrity. Sci. Rep. *8*, 11902. https://doi.org/10.1038/s41598-018-30355-3.

Buas, M.F., Kabak, S., and Kadesch, T. (2010). The Notch effector Hey1 associates with myogenic target genes to repress myogenesis. J. Biol. Chem. *285*, 1249–1258.

Calo, E., and Wysocka, J. (2013). Modification of enhancer chromatin: what, how, and why? Mol. Cell *49*, 825–837.

Chang, B., Hawes, N.L., Hurd, R.E., Davisson, M.T., Nusinowitz, S., and Heckenlively, J.R. (2002). Retinal degeneration mutants in the mouse. Vis. Res. *42*, 517–525. https://doi.org/10.1016/s0042-6989(01)00146-8.

Chen, S., Wang, Q.-L., Nie, Z., Sun, H., Lennon, G., Copeland, N.G., Gilbert, D.J., Jenkins, N.A., and Zack, D.J. (1997). Crx, a novel Otx-like paired-homeodomain protein, binds to and transactivates photoreceptor cell-specific genes. Neuron *19*, 1017–1030.

Chen, C.W., Koche, R.P., Sinha, A.U., Deshpande, A.J., Zhu, N., Eng, R., Doench, J.G., Xu, H., Chu, S.H., Qi, J., Wang, X., et al. (2015). DOT1L inhibits SIRT1-mediated epigenetic silencing to maintain leukemic gene expression in MLL-rearranged leukemia. Nat. Med. *21*, 335–343. https://doi.org/10.1038/nm.3832.

Cheng, F., Liu, J., Zhou, S.H., Wang, X.N., Chew, J.F., and Deng, L.-W. (2008). RNA interference against mixed lineage leukemia 5 resulted in cell cycle arrest. Int. J. Biochem. Cell Biol. *40*, 2472–2481.

Corbo, J.C., Lawrence, K.A., Karlstetter, M., Myers, C.A., Abdelaziz, M., Dirkes, W., Weigelt, K., Seifert, M., Benes, V., and Fritsche, L.G. (2010). CRX ChIP-seq reveals the cis-regulatory architecture of mouse photoreceptors. Genome Res. *20*, 1512–1525.

Deng, L.-W., Chiu, I., and Strominger, J.L. (2004). MLL 5 protein forms intranuclear foci, and overexpression inhibits cell cycle progression. Proc. Natl. Acad. Sci. U S A *101*, 757–762.

Deng, X., Iwagawa, T., Fukushima, M., Suzuki, Y., and Watanabe, S. (2021). Setd1a plays pivotal roles for the survival and proliferation of retinal progenitors via histone modifications of Uhrf1. Invest. Ophthalmol. Vis. Sci. *62*, 1. https://doi.org/10.1167/iovs.62.6.1.

Ding, X., Jiang, W., Zhou, P., Liu, L., Wan, X., Yuan, X., Wang, X., Chen, M., Chen, J., and Yang, J. (2015). Mixed lineage leukemia 5 (MLL5) protein stability is cooperatively regulated by O-GlcNac transferase (OGT) and ubiquitin specific protease 7 (USP7). PLoS One *10*, e0145023.

Emerling, B.M., Bonifas, J., Kratz, C.P., Donovan, S., Taylor, B.R., Green, E.D., Le Beau, M.M., and Shannon, K.M. (2002). MLL5, a homolog of Drosophila trithorax located within a segment of chromosome band 7q22 implicated in myeloid leukemia. Oncogene *21*, 4849–4854.

Feng, Q., Wang, H., Ng, H.H., Erdjument-Bromage, H., Tempst, P., Struhl, K., and Zhang, Y. (2002). Methylation of H3-lysine 79 is mediated by a new family of HMTases without a SET domain. Curr. Biol. *12*, 1052–1058. https://doi.org/10.1016/s0960-9822(02)00901-6.

Furukawa, T., Morrow, E.M., and Cepko, C.L. (1997). Crx, a novel otx-like homeobox gene, shows photoreceptor-specific expression and regulates photoreceptor differentiation. Cell *91*, 531–541.

Furukawa, T., Morrow, E.M., Li, T., Davis, F.C., and Cepko, C.L. (1999). Retinopathy and attenuated circadian entrainment in Crx-deficient mice. Nat. Genet. *23*, 466–470.

Guccione, E., Martinato, F., Finocchiaro, G., Luzi, L., Tizzoni, L., Dall'Olio, V., Zardo, G., Nervi, C., Bernard, L., and Amati, B. (2006). Myc-binding-site recognition in the human genome is determined by chromatin context. Nat. Cell Biol. *8*, 764–770.

Hamann, S., Métrailler, S., Schorderet, D.F., and Cottet, S. (2013). Analysis of the cytoprotective role of α-crystallins in cell survival and implication of the αA-crystallin C-terminal extension domain in preventing Bax-induced apoptosis. PLoS One *8*, e55372. https://doi.org/10.1371/journal.pone.0055372.

Hennig, A.K., Peng, G.-H., and Chen, S. (2008). Regulation of photoreceptor gene expression by Crx-associated transcription factor network. Brain Res. *1192*, 114–133.

Hsiau, T.H.-C., Diaconu, C., Myers, C.A., Lee, J., Cepko, C.L., and Corbo, J.C. (2007). The cis-regulatory logic of the mammalian photoreceptor transcriptional network. PLoS One *2*, e643.

Huang, Y.C., Shih, H.Y., Lin, S.J., Chiu, C.C., Ma, T.L., Yeh, T.H., and Cheng, Y.C. (2015). The epigenetic factor Kmt2a/Mll1 regulates neural progenitor proliferation and neuronal and glial differentiation. Dev. Neurobiol. *75*, 452–462.

Hubert, A., Henderson, J.M., Ross, K.G., Cowles, M.W., Torres, J., and Zayas, R.M. (2013). Epigenetic regulation of planarian stem cells by the SET1/MLL family of histone methyltransferases. Epigenetics *8*, 79–91.

Irie, S., Sanuki, R., Muranishi, Y., Kato, K., Chaya, T., and Furukawa, T. (2015). Rax homeoprotein regulates photoreceptor cell maturation and survival in association with Crx in the postnatal mouse retina. Mol. Cell. Biol. *35*, 2583–2596. https://doi.org/10.1128/MCB.00048-15.

Iwagawa, T., and Watanabe, S. (2019). Molecular mechanisms of H3K27me3 and H3K4me3 in

retinal development. Neurosci. Res. *138*, 43–48. https://doi.org/10.1016/j.neures.2018.09.010.

Lemak, A., Yee, A., Wu, H., Yap, D., Zeng, H., Dombrovski, L., Houliston, S., Aparicio, S., and Arrowsmith, C.H. (2013). Solution NMR structure and histone binding of the PHD domain of human MLL5. PLoS One *8*, e77020.

Ljungman, M., Parks, L., Hulbatte, R., and Bedi, K. (2019). The role of H3K79 methylation in transcription and the DNA damage response. Mutat. Res. *780*, 48–54. https://doi.org/10.1016/j.mrrev.2017.11.001.

Nguyen, A.T., and Zhang, Y. (2011). The diverse functions of Dot1 and H3K79 methylation. Genes Dev. *25*, 1345–1358. https://doi.org/10.1101/gad.2057811.

Nin, D.S., Huang, W., Ali, M., Yew, C.W., Kutateladze, T.G., and Deng, L.-W. (2015). O-GlcNAcylation of MLL5β is essential for MLL5β–AP-1 transcription complex assembly at the HPV16/18-long control region. J. Mol. Cell Biol. *7*, 180–183. https://doi.org/10.1093/jmcb/mjv009.

Peng, G.-H., and Chen, S. (2007). Crx activates opsin transcription by recruiting HAT-containing co-activators and promoting histone acetylation. Hum. Mol. Genet. *16*, 2433–2452.

Peterson, C.L., and Laniel, M.-A. (2004). Histones and histone modifications. Curr. Biol. *14*, R546–R551.

Popova, E.Y., Xu, X., DeWan, A.T., Salzberg, A.C., Berg, A., Hoh, J., Zhang, S.S., and Barnstable, C.J. (2012). Stage and gene specific signatures defined by histones H3K4me2 and H3K27me3 accompany mammalian retina maturation *in vivo*. PLoS One *7*, e46867.

Raeisossadati, R., Ferrari, M.F.R., Kihara, A.H., AlDiri, I., and Gross, J.M. (2021). Epigenetic regulation of retinal development. Epigenet. Chromatin *14*, 11. https://doi.org/10.1186/s13072-021-00384-w.

Rao, R.C., Tchedre, K.T., Malik, M.T.A., Coleman, N., Fang, Y., Marquez, V.E., and Chen, D.F. (2010). Dynamic patterns of histone lysine methylation in the developing retina. Invest. Ophthalmol. Vis. Sci. *51*, 6784–6792.

Ruzycki, P.A., Zhang, X., and Chen, S. (2018). CRX directs photoreceptor differentiation by accelerating chromatin remodeling at specific target sites. Epigenet. Chromatin *11*, 42. https://doi.org/10.1186/s13072-018-0212-2.

Sebastian, S., Sreenivas, P., Sambasivan, R., Cheedipudi, S., Kandalla, P., Pavlath, G.K., and Dhawan, J. (2009). MLL5, a trithorax homolog, indirectly regulates H3K4 methylation, represses cyclin A2 expression, and promotes myogenic differentiation. Proc. Natl. Acad. Sci. *106*, 4719–4724.

Shahbazian, M.D., Zhang, K., and Grunstein, M. (2005). Histone H2B ubiquitylation controls processive methylation but not monomethylation by Dot1 and Set1. Mol. Cell *19*, 271–277.

Solovei, I., Kreysing, M., Lanctôt, C., Kösem, S., Peichl, L., Cremer, T., Guck, J., and Joffe, B. (2009). Nuclear architecture of rod photoreceptor cells adapts to vision in mammalian evolution. Cell *137*, 356–368.

Steger, D.J., Lefterova, M.I., Ying, L., Stonestrom, A.J., Schupp, M., Zhuo, D., Vakoc, A.L., Kim, J.E., Chen, J., Lazar, M.A., Blobel, G.A., and Vakoc, C.R. (2008). DOT1L/KMT4 recruitment and H3K79 methylation are ubiquitously coupled with gene transcription in mammalian cells. Mol. Cell. Biol. *28*, 2825–2839. https://doi.org/10.1128/MCB.02076-07.

Sun, J., Zhao, Y., McGreal, R., Cohen-Tayar, Y., Rockowitz, S., Wilczek, C., Ashery-Padan, R., Shechter, D., Zheng, D., and Cvekl, A. (2016). Pax6 associates with H3K4-specific histone methyltransferases Mll1, Mll2, and Set1a and regulates H3K4 methylation at promoters and enhancers. Epigenet. Chromatin *9*, 37.

Swaroop, A., Kim, D., and Forrest, D. (2010). Transcriptional regulation of photoreceptor development and homeostasis in the mammalian retina. Nat. Rev. Neurosci. *11*, 563–576.

Tan, E., Ding, X.-Q., Saadi, A., Agarwal, N., Naash, M.I., and Al-Ubaidi, M.R. (2004). Expression of cone-photoreceptor–specific antigens in a cell line derived from retinal tumors in transgenic mice. Invest. Ophthalmol. Vis. Sci. *45*, 764–768.

Thompson, A.F., Crowe, M.E., Lieven, C.J., and Levin, L.A. (2015). Induction of neuronal morphology in the 661W cone photoreceptor cell line with staurosporine. PLoS One *10*, e0145270. https://doi.org/10.1371/journal.pone.0145270.

Tran, N.M., Zhang, A., Zhang, X., Huecker, J.B., Hennig, A.K., and Chen, S. (2014). Mechanistically distinct mouse models for CRX-associated retinopathy. PLoS Genet. *10*, e1004111.

Ueno, K., Iwagawa, T., Kuribayashi, H., Baba, Y., Nakauchi, H., Murakami, A., Nagasaki, M., Suzuki, Y., and Watanabe, S. (2016). Transition of differential histone H3 methylation in photoreceptors and other retinal cells during retinal differentiation. Sci. Rep. *6*, 29264.

Vlaming, H., and van Leeuwen, F. (2016). The upstreams and downstreams of H3K79 methylation by DOT1L. Chromosoma *125*, 593–605. https://doi.org/10.1007/s00412-015-0570-5.

Vogel, M.J., Guelen, L., de Wit, E., Hupkes, D.P., Lodén, M., Talhout, W., Feenstra, M., Abbas, B., Classen, A.-K., and van Steensel, B. (2006). Human heterochromatin proteins form large domains containing KRAB-ZNF genes. Genome Res. *16*, 1493–1504.

Vogel, M.J., Peric-Hupkes, D., and van Steensel, B. (2007). Detection of *in vivo* protein–DNA interactions using DamID in mammalian cells. Nat. Protoc. *2*, 1467–1478.

Wheway, G., Nazlamova, L., Turner, D., and Cross, S. (2019). 661W photoreceptor cell line as a cell model for studying retinal ciliopathies. Front. Genet. *10*, 308. https://doi.org/10.3389/fgene.2019.00308.

Woo Park, J., Kim, K.B., Kim, J.Y., Chae, Y.C., Jeong, O.S., and Seo, S.B. (2015). RE-IIBP methylates H3K79 and induces MEIS1-mediated apoptosis via H2BK120 ubiquitination by RNF20. Sci. Rep. *5*, 12485. https://doi.org/10.1038/srep12485.

Wood, K., Tellier, M., and Murphy, S. (2018). DOT1L and H3K79 methylation in transcription and genomic stability. Biomolecules *8*, 11. https://doi.org/10.3390/biom8010011.

Xue, Y., Shen, S.Q., Jui, J., Rupp, A.C., Byrne, L.C., Hattar, S., Flannery, J.G., Corbo, J.C., and Kefalov, V.J. (2015). CRALBP supports the mammalian retinal visual cycle and cone vision. J. Clin. Invest. *125*, 727–738. https://doi.org/10.1172/jci79651.

Yew, C.W., Lee, P., Chan, W.K., Lim, V.K.J., Tay, S.K., Tan, T.M., and Deng, L.-W. (2011). A novel MLL5 isoform that is essential to activate E6 and E7 transcription in HPV16/18-associated cervical cancers. Cancer Res. *71*, 6696–6707.

Zhang, X., Novera, W., Zhang, Y., and Deng, L.-W. (2017). MLL5 (KMT2E): structure, function, and clinical relevance. Cell. Mol. Life Sci. *74*, 2333–2344.

Zhao, W., Liu, J., Zhang, X., and Deng, L.-W. (2016). MLL5 maintains spindle bipolarity by preventing aberrant cytosolic aggregation of PLK1. J. Cell Biol. *212*, 829–843. https://doi.org/10.1083/jcb.201501021.

Zhou, P., Wang, Z., Yuan, X., Zhou, C., Liu, L., Wan, X., Zhang, F., Ding, X., Wang, C., and Xiong, S. (2013). Mixed lineage leukemia 5 (MLL5) protein regulates cell cycle progression and E2F1-responsive gene expression via association with host cell factor-1 (HCF-1). J. Biol. Chem. *288*, 17532–17543.

Zhou, P., Ding, X., Wan, X., Liu, L., Yuan, X., Zhang, W., Hui, X., Meng, G., Xiao, H., and Li, B. (2018). MLL5 suppresses antiviral innate immune response by facilitating STUB1-mediated RIG-I degradation. Nat. Commun. *9*, 1243.

Zhou, B., Fang, L., Dong, Y., Yang, J., Chen, X., Zhang, N., Zhu, Y., and Huang, T. (2021). Mitochondrial quality control protects photoreceptors against oxidative stress in the H(2)O(2)-induced models of retinal degeneration diseases. Cell Death Dis. *12*, 413. https://doi.org/10.1038/s41419-021-03660-5.

STAR★METHODS

KEY RESOURCES TABLE

REAGENT or RESOURCE	SOURCE	IDENTIFIER
Antibodies		
MLL5 Rabbit PolyAb	Zhao et al. (2016)	N/A
α tubulin Mouse mAb	Santa Cruz	Cat# sc-5286; RRID:AB_628411
GAPDH Rabbit PolyAb	Santa Cruz	Cat# sc-25778; RRID:AB_10167668
H3K4me1 Rabbit PolyAb	Abcam	Cat# ab8895; RRID:AB_306847
H3K4me2 Rabbit mAb	Abcam	(Cat# ab32356; RRID:AB_732924
H3K4me3 Mouse mAb	Abcam	Cat# ab1012; RRID:AB_442796
H3 Rabbit mAb	Cell Signaling Technology	Cat# 12648; RRID:AB_2797978
PKCα Mouse mAb	Santa Cruz	Cat# sc-8393; RRID:AB_628142
Rho Mouse mAb	Abcam	Cat# ab5417; RRID:AB_304874
Opn1mw Goat PolyAb	Santa Cruz	Cat# sc-22117; RRID:AB_2300956
Flag Mouse mAb	Sigma-Aldrich	Cat# F3165; RRID:AB_259529
Flag Rabbit PolyAb	Sigma-Aldrich	Cat# F7425; RRID:AB_439687
HA Mouse mAb	Sigma-Aldrich	Cat# H9658; RRID:AB_260092
β-Actin Rabbit PolyAb	ABclonal	Cat# AC006; RRID:AB_2768236
CRX Rabbit PolyAb	Santa Cruz	Cat# sc-30150; RRID:AB_2276566
CRX Mouse mAb	Abnova	Cat# H00001406-M02; RRID:AB_606098
Calbindin Mouse mAb	Sigma-Aldrich	Cat# C9848; RRID:AB_476894
Pax6 Rabbit PolyAb	Millipore	Cat# AB2237; RRID:AB_1587367
Chx10 Mouse mAb	Santa Cruz	Cat# sc-365519; RRID:AB_10842442
RNA polymerase II Rabbit PolyAb	Santa Cruz	Cat# sc-9001; RRID:AB_2268548
CBP Rabbit PolyAb	Santa Cruz	Cat# sc-369; RRID:AB_631006
H4Ac Rabbit PolyAb	Millipore	Cat# 06-866; RRID:AB_310270
GFP Mouse mAb	Abcam	Cat# ab1218; RRID:AB_298911
normal mouse IgG	Santa Cruz	Cat# sc-2025; RRID:AB_737182
normal rabbit IgG	Santa Cruz	Cat# sc-2027; RRID:AB_737197
Anti-rabbit IgG, HRP	Abcam	Cat# ab6721; RRID:AB_955447
Anti-mouse IgG, HRP	Abcam	Cat# ab6728; RRID:AB_955440
Goat anti-mouse IgG (H + L), Alexa Fluor 488	Molecular Probes	Cat# A-11029; RRID:AB_138404
Goat anti-rabbit IgG (H + L), Alexa Fluor 488	Molecular Probes	Cat# A-11008; RRID:AB_143165
Goat anti-rabbit IgG (H + L), Alexa Fluor 568	Molecular Probes	Cat# A-11011; RRID:AB_143157
Goat anti-mouse IgG (H + L), Alexa Fluor 568	Molecular Probes	Cat# A-11031; RRID:AB_144696
Donkey anti-goat IgG (H + +L), Alexa Fluor 568	Molecular Probes	Cat# A-11057; RRID:AB_142581
Chemicals, peptides, and recombinant proteins		
FITC conjugate PNA	Sigma-Aldrich	L7381
Polybrene	Sigma-Aldrich	TR-1003-G
Geneticin	Gibco	10131035
Puromycin	Gibco	A1113803
TRIzol	Invitrogen	155967-026
Protease Plus	ACD	322331
MLL5 RNAscope probe	ACD	575421

(*Continued on next page*)

Continued

REAGENT or RESOURCE	SOURCE	IDENTIFIER
Critical commercial assays		
SuperScript III RT-PCR system	Invitrogen	18080-051
iTaq universal SYBR green supermix	Bio-Rad	172-5120
One Shot™ Gateway PCR Cloning System	Invitrogen	12535029
Pfx DNA polymerase	Invitrogen	11708
RNAiMAX Lipofectamine	Invitrogen	13667-150
True Blot anti mouse IgG IP beads	eBioscience	00-8811-25
True Blot anti rabbit IgG IP beads	eBioscience	00-8800-25
RNAscope 2.5 HD Detection Kit-Brown	ACD	322310
RNeasy mini kit	Qiagen	74104
Dual-luciferase assay system	Promega	E1910
EpiQuikTM chromatin immunoprecipitation kit	Epigentek	P-2002
DNeasy Tissue kit	Qiagen	69504
Advantage cDNA polymerase mix	Clontech	639105
Deposited data		
Unprocessed western blot data and processed RNA-seq data	Mendeley Data	https://doi.org/10.17632/8vpy42r34y.1
Raw RNA-seq datasets	GEO	GSE196935
Experimental models: Cell lines		
661W cell line	Tan et al. (2004)	RRID:CVCL_6240
HEK293FT cell line	ATCC	RRID:CVCL_6911
HEK293T cell line	ATCC	RRID:CVCL_0063
Experimental models: Organisms/strains		
Mll5-KO mouse	Zhou et al. (2018)	N/A
Recombinant DNA		
Plasmid: pLgw-V5-EcoDam	Addgene	59210
Plasmid: pLgw-RFC1-V5-EcoDam	Addgene	59205
Plasmid: pLgw-MLL5-V5-EcoDam	This paper	N/A
Plasmid: pGL3-basic	Promega	U47295
Plasmid: pGL3-basic-Rho	This paper	N/A
Plasmid: pGL3-basic-Opn1mw	This paper	N/A
Plasmid: pGL3-basic-Opn1sw	This paper	N/A
Plasmid: pEF6	Invitrogen	K9610-20
Plasmid: pEF6-MLL5-PS	Zhao et al. (2016)	N/A
Plasmid: pEF6-MLL5-CD	Zhao et al. (2016)	N/A
Plasmid: pEF6-MLL5-CT	Zhao et al. (2016)	N/A
Plasmid: pEF6-MLL5-CD4	Zhao et al. (2016)	N/A
Plasmid: pEF6-MLL5-ΔCD4	This paper	N/A
Plasmid: pLenti-CMV-Puro	Addgene	17448
Plasmid: pLenti-CMV-Puro-MLL5-ΔCD4	This paper	N/A
Plasmid: pLenti-puro-Flag-MLL5	This paper	N/A
Plasmid: pLenti-puro-dest	Addgene	17293
Plasmid: pLenti-puro-Flag-MLL5-WT	This paper	N/A
Plasmid: pLenti-puro-Flag-MLL5-W141A	This paper	N/A

(*Continued on next page*)

Continued

REAGENT or RESOURCE	SOURCE	IDENTIFIER
Plasmid: pLenti-puro-Flag-MLL5-T440A	This paper	N/A
Plasmid: pXJ40-HA-CRX	This paper	N/A
Plasmid: pMSCVneo-HA-CRX-IRES-GFP	This paper	N/A
Plasmid: pLKO.1 puro	Addgene	8453
Plasmid: pLKO.1 puro-MLL5 shRNA	Zhao et al. (2016)	N/A
Plasmid: pLenti-puro-dest	Addgene	17293
Plasmid: pCMV-ΔR8.91	Lifescience Market	PVT2323
Plasmid: PMD2.G	Addgene	12259
Plasmid: PCL-Eco	Addgene	12371
Plasmid: VSV-G	Addgene	138479
Plasmid: Gag-Pol	Addgene	14887
Software and algorithms		
FLU OVI EW viewer software	Olympus	Ver. 4.2
Ganzfeld dome stimulating and data collecting system	Roland Consult	Q450SC UV
GraphPad Prism	GraphPad	6.01

RESOURCE AVAILABILITY

Lead contact

Lih-Wen Deng (bchdlw@nus.edu.sg)

Materials availability

Plasmids generated in this study are available upon request from the lead contact, Lih-Wen Deng (bchdlw@nus.edu.sg), but a completed Materials Transfer Agreement may be required.

Data and code availability

Raw sequencing reads have been deposited to GEO: GSE196935. The accession number is also listed in the key resources table. Original western blot images and processed RNA-seq data have been deposited at Mendeley. The DOI is listed in the key resources table.

This paper does not contain original code.

Any additional information required to reanalyze the data reported in this paper is available from the lead contact upon request.

EXPERIMENTAL MODEL AND SUBJECT DETAILS

Mice

Mll5-KO mouse was generated as previously described (Zhou et al., 2018). Mice were housed in a temperature-controlled room at 24°C with a 12 h light/dark cycle. Fresh water and rodent diet were continuously available. *Mll5*-WT and *Mll5*-KO mice used in this study were littermates with same sex on C57BL/6J background at ages indicated in specific experiments. Specifically, ERG was performed with female mice at the age of P16. RNA-seq, qPCR, co-IP and qChIP were performed with P18 female mice retinas, while ISH and immunostaining were performed with P21 male mice retinas. All experimental procedures conformed to the ARVO statement for the Use of Animals in Ophthalmic and Vision Research, and were approved by the Institutional Animal Care and Use Committee (IACUC) of NUS (Singapore), City University of Hong Kong (Hong Kong, China) and Wenzhou Medical University (Wenzhou, China).

METHOD DETAILS

Cell culture

The murine photoreceptor-derived 661W cell line was a kind gift from Dr. Muayyad R. Al-Ubaidi (Department of Cell Biology, University of Oklahoma Health Sciences Center, Oklahoma City, OK, USA). 661W cells, embryonic kidney cell line HEK293FT, and HEK293T cells were maintained in DMEM containing 10% FBS and 2 mM L-glutamine at 37°C under a humidified atmosphere of 5% CO_2.

siRNA transfection and plasmid constructions

MLL5-specific siRNA duplexes #1 (sense: 5′-TGCTGAGAGAACAGTTTGA-3′; anti-sense: 5′-TCAAAC TGTTCTCTCAGCA-3′) and #2 (sense: 5′-CAGCCCTCTGCAA ACTTTCAGAATT-3′; anti-sense: 5′-AATTCT GAAAGTTTGCAGAGGGCTG-3′) targeting nucleotide position 1,088 and 4,693 respectively from the translation starting point of murine MLL5 (National Center for Biotechnology Information (NCBI) reference sequence: NM_026984.1) were generated from 1st BASE (Singapore). Scrambled siRNA was designed as previously described (Yew et al., 2011). siRNAs were transfected into cells using RNAiMAX Lipofectamine (13667-150; Invitrogen) following the manufacturer's instructions. MLL5-specific shRNA targeting nucleotide position at 1,556 from the transcription starting point of human MLL5, and scrambled shRNA were cloned into the pLKO.1 puro vector (Addgene #8453) with *Age1* and *EcoR1* sites as previously described (Deng et al., 2004; Zhao et al., 2016). N-terminal Flag-tagged human MLL5 and its deletion mutants, including MLL5-PS, MLL5-CD, MLL5-CT, MLL5-CD4 were previously cloned into the pEF6 vector (K9610-20; Invitrogen) (Zhao et al., 2016). Flag-MLL5-ΔCD4 was generated by flanking two PCR fragments of human MLL5 cDNA (nucleotides 1-2454 and 3451-5604), using the *Asc1* restriction enzyme recognition sequence, and cloning into the pEF6 vector using *BamH1* and *Not1* sites. Flag-MLL5-ΔCD4 was also cloned into pLenti-CMV-Puro (#17448; Addgene) vector with *Xba1* and *BamH1* sites. The N-terminal HA-tagged cDNA sequence encoding murine CRX (CCDS20840.1) was synthesized from murine retinal RNA using the SuperScript III RT-PCR system (Invitrogen) and cloned into the pXJ40 vector with *Not1* and *Kpn1* sites. To generate constructs for viral packages, the HA-CRX construct was digested with *Not1* and fused to the N-terminus of the pMSCVneo-IRES-GFP vector to generate pMSCVneo-HA-CRX-IRES-GFP, whereas N-terminal Flag-tagged human MLL5 amplicons were cloned into a lentiviral vector using Gateway cloning. Briefly, Flag-MLL5 was first cloned into the Gateway entry vector pDONR 221 (Invitrogen) using BP Clonase II (11789; Invitrogen). The resulting entry plasmid was then recombined with the lentiviral destination vector, pLenti-puro-dest (#17293; Addgene) using LR Clonase II (11791; Invitrogen). For the construction of siRNA-resistant MLL5, two base mutations (G1092-A1093 mutated to A1092-C1093) were introduced into the wide-type pLenti-puro-Flag-MLL5 plasmid within the 19-bp MLL5-siRNA targeting sequence by PCR using Pfx DNA polymerase (11708; Invitrogen). Domain mutant constructs were generated in a similar manner with appropriately designed primers (Table S2). The pLgw-MLL5-V5-EcoDam plasmid for the DamID experiments was generated by Gateway recombination of pDONR 221-MLL5 with the lentiviral destination vector pLgw-RFC1-V5-EcoDam using LR Clonase II. DamID lentiviral vectors, pLgw-V5-EcoDam and pLgw-RFC1-V5-EcoDam, were kindly provided by Dr Bas Van Steensel (Netherlands Cancer Institute). To generate constructs for the luciferase assay, a 1510-bp fragment containing the distal and proximal promoter of human *Rho* gene (nucleotides -1500 to +10) was cloned into pGL3-basic (U47295; Promega) vector with *NheI* and *HindIII* sites. Similarly, 1.5-kb upstream genomic fragments of the murine *Opn1mw* gene (-1441 to -14) and *Opn1sw* gene (-1450 to -11) were subcloned into the PGL3-basic vector to generate *MmOpn1mw* and *MmOpn1sw* luciferase reporter plasmids. All constructs generated by PCR were verified by sequencing. All viral transfer plasmids were amplified in *Stbl3* competent cells.

RNA extraction, cDNA synthesis, and quantitative PCR (qPCR)

661W cell pellets or retinas dissected from *Mll5*-WT or *Mll5*-KO mice at the indicated ages were homogenised using TRIzol reagent (155967-026; Invitrogen), followed by chloroform-isopropanol-alcohol extraction for total RNA. Two micrograms of total RNA were then reverse transcribed to cDNA using the SuperScript III RT-PCR system (18080-051; Invitrogen). cDNA was diluted and quantified using iTaq universal SYBR green supermix (172-5120; Bio-Rad Laboratories) with an iQ5 Multicolor Real-Time PCR machine (Bio-Rad Laboratories). Primers are listed in Table S2. Relative expression was determined from three independent experiments with three repeats for each experiment and analysed by student t-test.

Immunoprecipitation (IP) and Western blotting

To monitor MLL5 and CRX association by co-IP, retinas dissected from P18 mice were homogenized in a glass homogenizer and lysed in a buffer containing 150 mM NaCl, 50 mM Tris-HCl, pH 8.0, 0.5% NP-40,

0.05% SDS, and protease inhibitors (2 mM PMSF, 2 μg/mL leupeptin, 2 μg/mL aprotinin, 1 μg/mL pepstatin A, 1 mM Na_3VO_4, 5 mM NaF, and 10 mM β-glycerophosphate). To dissect which domain of MLL5 interacts with CRX, HEK293T cells cultured in 60-mm dishes were sequentially transfected with pXJ40-HA-CRX plasmids (4 μg) and pEF6-Flag-MLL5 (8 μg) or pEF6-Flag-MLL5-PS/-CD/-CT/-CD4/-ΔCD4 (4 μg). Cells were harvested 48 h after transfection and lysed with 1 mL lysis buffer for 15 min on ice. Lysates were then centrifuged at 12,000 *g* for 10 min, pre-cleared with anti-Mouse/Rabbit Ig IP Beads (Rockland Immunochemicals) for 30 min, and incubated with 2 μg anti-MLL5 antibody, anti-CRX antibody, anti-Flag antibody, or anti-HA antibody for 3 h, followed by a 2 h incubation with 10 μL of anti-Mouse/Rabbit Ig IP Beads. The protein-bound beads were rinsed four times with cell lysis buffer, eluted with 2xLaemmli sample buffer containing 200 mM DTT, and analysed by western blotting. Luminescent signals were captured using the ChemiDoc™ Imaging System and quantified by ImageJ software. To prepare direct lysates for western blotting, tissues or cells were harvested and rinse twice with ice-cold PBS, and lysed with RIPA buffer supplied with proteinase inhibitors. Tissues or cells were then sonicated at 20% amplitude on ice with a Vibra-Cell sonicator until they were fully lyzed. The lysates were then incubated on ice for 10 min and centrifuged at 12,000 *g* for 10 min. The supernatants were then transferred to new tubes and measured protein concentration with Bradford assay, denatured with 2× Laemmli sample buffer containing 200 mM DTT. An equal amount of protein (10 μg) was used for western blotting analysis.

Histology and immunohistochemistry

Whole eyeballs were dissected and fixed in Davidson's fixative buffer (0.8% PFA, 35% ethanol, and 10% glacial acetic acid) overnight. After rinsing with PBS, eyeballs were subjected to dehydration through increasing concentration of ethanol and xylene, followed by embedding into paraffin. Five-micron paraffin sections were generated on a Leica RM2235 microtome and mounted onto slides. Sections were then rehydrated through decreasing concentration of ethanol (100%, 95%, 70%, and 50%) and subsequently stained with haematoxylin and eosin (H&E) for morphological assessments or used for immunohistochemistry. For immunohistochemistry, sections were permeabilised in 0.5% Triton X-100 in PBS for 15 min after antigen retrieval, and then incubated in blocking buffer (5% BSA in PBS) for 2 h. After incubation with primary antibodies in blocking buffer overnight at 4°C, sections were then incubated with secondary antibodies for 2 h at room temperature (RT). Images were obtained using a confocal fluorescence microscope FV 1000 (Olympus) equipped with a built-in laser scanning unit, using FLU OVI EW viewer software (Ver. 4.2; Olympus).

Mouse retina *in situ* hybridization

In situ hybridization using RNAscope probes was performed following the manufacturer's protocol for RNAscope 2.5 HD Detection Kit-Brown (ACD, Catalog No. 322310). Briefly, eyeballs dissected from P21 mice were fixed in fresh 10% Neutral buffered formalin for 24 h at RT, dehydrated, and embedded in paraffin. 5μm eyeball sections were baked, deparaffinized and air dry for 5min, followed by incubation in hydrogen peroxide for 10 min at RT. After target retrieval by boiling in target retrieval buffer for 15 min, slides were briefly washed with distilled water and pre-treated by incubation with Protease Plus (ACD, Catalog No. 322331) for 30 min at 40°C. After that, the manufacturer's protocol for RNAscope 2.5 assay was followed exactly to hybridize probes and detect the signals. RNAscope probe used for *Mll5* detection was designed to target nucleotide position 436-1591 of murine MLL5 (ACD, Catalog No. 575421).

Focal electroretinogram (fERG)

Scotopic and photopic responses in both eyes of an individual mouse were recorded with a well-established Ganzfeld dome stimulating and data collecting system (Q450SC UV; Roland, Wiesbaden, Germany). Briefly, mice were dark-adapted for 6 h and subsequently anaesthetised with an intraperitoneal injection of a mixture of ketamine (72 mg/kg) and xylazine (4 mg/kg). Pupils were then dilated with 1% atropine and 2.5% phenylephrine hydrochloride before the experiment. Ground electrodes and a referential needle were punctured into the tail and cheek, respectively. The mice were then stimulated with five levels of stimuli ranging from 3.0 to -1.7 log cd-s/m^2 to elicit scotopic ERGs. After 10 min of light adaption with a background light of 5 log cd-s/m^2, the mice were then subjected to photopic ERG measurement upon stimulation with five levels of stimuli ranging from 0.7 to 3.3 log cd-s/m^2.

RNA-seq

For the preparation of total RNA for RNA-seq, 8 eyeballs of two pairs of female *Mll5*-WT and *Mll5*-KO mice at the age of P18 were dissected. Total RNA was extracted with RNeasy mini kit (Qiagen, 74104).

A minimum of 2 μg of total RNA obtained from mixture of 2 eyeballs were used for library construction, and the remining RNA were used for cDNA synthesis and qPCR analysis. Library sequencing was performed on the Illumina HiSeq-PE150 platform. RNA-seq results from two experimental repeats were presented.

Virus production and transduction

Lentivirus production was performed as previously described (Zhao et al., 2016) with the following modifications. HEK293FT cells cultured in 60-mm dishes were co-transfected with lentiviral transfer constructs (pLenti-puro-Flag-MLL5-WT/-W141A/-T440A, pLenti-puro-empty, pLgw-MLL5-V5-EcoDam, or pLgw-V5-EcoDam; 4 μg), packaging construct pCMV-ΔR8.91 (encoding the HIV-1 gag-pol; 2 μg), along with PMD2.G (encoding the VSV-G envelope; 0.4 μg) using the calcium phosphate method. The lentivirus-containing supernatant was harvested on three consecutive days and concentrated. For the production of retrovirus for 661w transduction, the procedure above was performed, except that transfection plasmids were pMSCVneo-HA-CRX-IRES-GFP or pMSCVneo-empty (4 μg), together with PCL-Eco (2.0 μg), VSV-G (1.0 μg), and Gag-Pol plasmids (1.0 μg). After transfection, the virus-containing cell supernatant was diluted in DMEM complete medium in the presence of 8 μg/mL polybrene and added to 661W cells. After 24 h incubation, medium was replaced with fresh culture medium and incubated for a further 48 h. Cells were then subjected to selection using 2.5 μg/mL puromycin or 2 mg/mL G418 selection for 24 h before harvesting.

Dual-luciferase assay

To measure the transcription activity of *HsRho*, *MmOpn1mw*, and *MmOpn1sw* promoters, HEK293T cells in 24-well plates were transfected with pEF6-Flag-MLL5 or pEF6-Flag empty plasmid (0.6 μg), followed by a subsequent transfection with pGL3-Rho promoter-Luc plasmids (0.4 μg) together with pXJ40-HA-CRX DNA (0.4 μg) and pRL-TK-Renilla luciferase expression vector (0.1 μg) using a standard calcium phosphate method. Depletion of endogenous MLL5 expression in HEK293T cells was achieved by transfection of shRNA duplexes, using the calcium phosphate method. Each plasmid combination was transfected in duplicate. Cells were harvested 48 h post-transfection for western blotting and luciferase assays. Relative luminometer units (RLU) result from Firefly luciferase reaction and Renilla luciferase reaction were measured with a Dual-luciferase assay system (E1910; Promega) on a Synergy H1 microplate reader (Bio-Tek). Each firefly luciferase RLU was normalised to the control Renilla luciferase RLU, and was presented as relative fold change compared to negative controls.

Chromatin immunoprecipitation (ChIP) analysis

An EpiQuikTM chromatin immunoprecipitation kit (P-2002) from Epigentek Group Inc. (Brooklyn, NY) was used following the manufacturer's protocol. Briefly, P18 mouse retinas were dissected in ice-cold PBS prior to homogenisation and crosslinking. Chromatin was sonicated to obtain sheared DNA fragments of 200-1000-bp in length. One microgram of antibody was used per immunoprecipitation (IP) from approximately 2 million retinal cells or 661W (CRX OE) cells. DNA from precipitated chromatin and input controls were analysed by qPCR using specific primers for the promoter or 3′ UTR regions of the *Rho* gene, as well as primers for *Collagenase* gene promoter. A pair of primers recognising a region of chromosome 8 that does not contain any histone modifications was included as a negative control. All qPCR primer sequences are described in Table S2. The difference was calculated as: % Input = 2^ [Input Ct – (log x)/ (log2)-ChIP Ct] *100%, where "x" is the ratio of ChIP sample volume to Input sample volume.

DamID assay

DamID was performed as previously described (Vogel et al., 2007). Briefly, 661W (EV OE) and 661W (CRX OE) cells were incubated overnight with lentivirus expressing MLL5-Dam or Dam-control proteins and then cultured for another 48 h before subjected to selection using 2 mg/mL G418 for 24 h. Cells were then subjected to a standard DamID protocol (Vogel et al., 2006). Briefly, genomic DNA was extracted using the DNeasy Tissue kit (Qiagen). Genomic DNA (2.5 μg) was digested with *DpnI* and ligated to adaptors, followed by *DpnII* digestion. GATC methylated DNA was then amplified by ligation-mediated PCR with Advantage cDNA polymerase mix (639105; Clontech). Amplicons were purified and subjected to quantitative PCR analysis with gene-specific primers (Table S2).

QUANTIFICATION AND STATISTICAL ANALYSIS

All statistical analyses were performed using GraphPad Prism 6.01. Significance levels were obtained by student t test and indicated by *$p < 0.05$, **$p < 0.01$, ***$p < 0.001$, ns (not significant when $p \geq 0.05$). Error bars represent the SEM of three independent experiments.